

Single-molecule fluorescence multiplexing by multi-parameter spectroscopic detection of nanostructured FRET labels

Jiachong Chu^{1*}, Ayesha Ejaz^{2*}, Madeline R. Joseph¹, Aria E. Coraor¹, Kyle M. Lin^{3,4}, and Allison H. Squires^{1,5△}

¹Pritzker School of Molecular Engineering, University of Chicago, IL, USA

²Department of Chemistry, University of Chicago, IL, USA

³Graduate Program in Biophysical Sciences, University of Chicago, Chicago, IL, USA

⁴Medical Scientist Training Program, Pritzker School of Medicine, University of Chicago, Chicago, IL, USA

⁵Institute for Biophysical Dynamics, University of Chicago, Chicago, IL, USA

*Authors contributed equally to this work

△e-mail correspondence: asquires@uchicago.edu

Abstract

Multiplexed, real-time fluorescence detection at the single-molecule level is highly desirable to reveal the stoichiometry, dynamics, and interactions of individual molecular species within complex systems. However, traditionally fluorescence sensing is limited to 3-4 concurrently detected labels, due to low signal-to-noise, high spectral overlap between labels, and the need to avoid dissimilar dye chemistries. To surmount these barriers, we have engineered a palette of several dozen fluorescent labels, called FRETfluors, for spectroscopic multiplexing at the single-molecule level. Each FRETfluor is a compact nanostructure formed from the same three chemical building blocks (DNA, Cy3, and Cy5). The composition and dye-dye geometries create a characteristic Förster Resonance Energy Transfer (FRET) efficiency for each construct. In addition, we varied the local DNA sequence and attachment chemistry to alter the Cy3 and Cy5 emission properties and thereby shift the emission signatures of an entire series of FRET constructs to new sectors of the multi-parameter detection space. Unique spectroscopic emission of each FRETfluor is therefore conferred by a combination of FRET and this site-specific tuning of individual fluorophore photophysics. We show single-molecule identification of a set of 27 FRETfluors in a sample mixture using a subset of constructs statistically selected to minimize classification errors, measured using an Anti-Brownian ELectrokinetic (ABEL) trap which provides precise multi-parameter spectroscopic measurements. The ABEL trap also reveals transport properties of a trapped particle, which enables discrimination between FRETfluors attached to a target (here: mRNA) and unbound FRETfluors, eliminating the need for washes or removal of excess label by purification. We show single-molecule identification of a set of 27 FRETfluors in a sample mixture using a subset of constructs selected to minimize classification errors. Although usually considered an undesirable complication of fluorescence, here the inherent sensitivity of fluorophores to the local physicochemical environment provides a new design axis that is nearly orthogonal to changing the geometry of a FRET construct. As a result, the number of distinguishable FRET-based labels can be combinatorically expanded while maintaining chemical compatibility, opening up new possibilities for spectroscopic multiplexing at the single-molecule level using a minimal set of chemical components.

Introduction

Multiplexed measurements provide critical insights into the molecular compositions and interactions that govern complex nanoscale systems. Fluorescent labels offer highly sensitive and specific readout of molecular identity, enabling information-rich imaging and assays with a rainbow of colors for microscale objects.^{1,2} At the single-molecule level, color ratio-based multiplexing has been demonstrated by multiple groups for up to ~10 labels exhibiting unique color combinations,³ by advanced data processing, and very recently up to 25 labels with four-laser alternating excitation and four dyes.⁴ However, low signal-to-noise ratios and overlapping spectra generally restrict single-molecule fluorescence multiplexing to at most 3-4 colors⁵. Ultimately, prospects for color ratio-based multiplexing remain limited at the single-molecule level.

To overcome these limitations, technologies for single-molecule fluorescence multiplexing must utilize additional measurement dimensions to separate signals. Chemical fixation and surface immobilization of samples enable elegant multiplexing strategies for up to thousands of labels via barcoding approaches where unique combinations of molecular interactions are detected through multiple rounds of readout for each molecule, providing patterning in temporal⁶⁻⁸, spatial⁹⁻¹³, or kinetic¹⁴⁻¹⁶ dimensions. For living or dynamic samples, however, multiplexing must be encoded in additional spectroscopic dimensions for each fluorescent label without the aid of temporal or spatial patterning, since repeated measurements of the same molecule cannot be guaranteed.¹⁷ Spectroscopic properties including fluorescence brightness and quantum yield, fluorescence lifetime, anisotropy, and emission spectrum are routinely accessible with single-molecule sensing methods.¹⁸⁻²² By labeling samples with a variety of fluorophores that possess different photophysical properties, spectroscopically multiplexed imaging at or approaching the single molecule level has been demonstrated using up to nine labels,²³ and other sensing modalities have achieved up to six labels in complex sample mixtures with different fluorophores.^{3,24} But although use of chemically diverse fluorophores offers a potentially broad spectroscopic palette, the number of labels that can be concurrently identified is ultimately constrained by dissimilar chemical compatibility and labeling performance across different chemical structures.

One well-established means to generate a variety of spectroscopic signals using a limited number of compounds is Förster Resonance Energy Transfer (FRET) for fluorophores positioned on DNA nanostructures.²⁵⁻²⁷ The pairwise rate of energy transfer between an excited donor and a potential acceptor is influenced by the photophysical properties of both fluorophores and by their relative geometry, including spatial separation and orientation.^{5,28} DNA nanotechnology is a powerful tool for engineering FRET networks because it can be used to create molecular scaffolds that position and orient covalently linked fluorophores with sub-nanometer precision,^{9,29} governing the flow of energy through the structure and thereby dictating the observed spectroscopic properties.³⁰⁻³² (Note that many barcoding-based single-molecule fluorescence multiplexing approaches also employ DNA-fluorophore constructs to achieve spatial or interaction patterning.) For a single FRET pair (one donor, one acceptor) on a simple DNA scaffold, spectroscopic multiplexing of several DNA constructs³³ and up to as many as 15 constructs,³⁴ has been demonstrated at the single-molecule level. In principle, these numbers could be increased using more complex DNA-FRET constructs, or constructs with additional donors, acceptors, or fluorophore types. However, practical limitations of DNA-FRET constructs for multiplexing must be considered, including the typical spatial extent of FRET interactions (~10 nm) and tradeoffs among scaffold complexity, spectroscopic uniqueness, and error-free assembly and readout. Moreover, emission from a FRET network reflects tight coupling among spectroscopic properties due to underlying

physical processes, so commonly measured variables such as donor lifetime and brightness, FRET efficiency, emission spectrum, and acceptor brightness show correlated or anticorrelated variation across different constructs.⁵

Dyes attached to DNA are sensitive to changes in local base sequence and attachment chemistries, both of which influence the local physicochemical environment by changing structural flexibility and conformations as well as solvent accessibility and interactions with the DNA scaffold.³⁵ Cyanine dyes on DNA are a particularly well-studied class of constructs in this context,³⁶ and exhibit changing lifetimes and quantum yields,^{37–40} orientation and base stacking,^{27,41–43} system-bath coupling,⁴⁴ and torsion and isomerization.^{45–47} Naturally, such photophysical changes also influence energy transfer on DNA-FRET nanostructures.^{37,44}

Here we demonstrate that engineered photophysical modifications can be incorporated into DNA-FRET constructs to facilitate spectroscopic multiplexing at the single-molecule level. We have designed a set of labels, called “FRETfluors”, which produce unique spectroscopic signatures from different configurations of three simple building blocks (DNA, Cy3, and Cy5). Energy transfer between the donor (Cy3) and acceptor (Cy5), in combination with the effects of local DNA sequence and attachment chemistry, tunes the spectroscopic emission of each FRETfluor across multiple measurable parameters including color, brightness, and fluorescence lifetime. Readout in an Anti-Brownian ELectrokinetic (ABEL) trap^{48–52} provides high-precision multiparameter measurements for FRETfluors in solution at 5 pM concentration. Pairwise comparison of the characteristic emission parameters observed for each FRETfluor allows statistically optimal subsets to be selected for multiplexing. We show sequence-specific labeling of both DNA and mRNA with FRETfluors, and show that it is not necessary to wash or purify out excess labels that have not found a target, because the ABEL trap reliably discriminates between target-bound and free FRETfluors.^{34,53} Finally, we show single-molecule identification of a set of 27 FRETfluor labels in a sample mixture, illustrating that the combination of FRET and tuning fluorophore photophysics provides new opportunities for signal multiplexing from a minimal set of chemical components.

Design of FRETfluor labels

We sought to create a collection of fluorescent labels with unique spectroscopic signals, high chemical homogeneity, and minimal structural complexity. FRETfluors use a minimal set of biomolecular building blocks: DNA oligomers functionalized with either Cy3 or Cy5 dye (see Supplementary Table S1 for sequences). We first created a series of constructs incorporating non-sulfonated Cy3 and Cy5 into the DNA backbone as shown in Fig. 1a. Cy3 is positioned in the “A” strand (cyan), with N basepairs (here: 9 bp) separating it from the Cy5 positioned in the “B” strand (blue). Hereafter these constructs are referred to as “ABN” (here: AB9). We chose phosphoramidite incorporation of dyes into the DNA backbone to limit dipole rotational mobility³⁸ and to improve photostability.⁵⁴ Other ABN FRETfluors have Cy3 in the same location, with Cy5 placed closer or farther for $6 \leq N \leq 20$ (spacing between 2 and 7 nm). A “bridge” strand (green) hybridizes to the 3’ end of the A strand, with an overhang whose sequence can be tuned to match a target nucleic acid, enabling sequence-specific labeling of the target. The single-exponential fitted lifetime and background-subtracted brightness of the Cy3 donor in an ABN

complex lacking Cy5 (AB0 construct) were measured to be $\tau_{AB0} = 1.6 \pm 0.03$ ns, green brightness 0.31 ± 0.012 counts $\text{ms}^{-1} \mu\text{W}^{-1}$.

Although FRET can be used to tune the emission profile across a set of fluorophores, the resulting spectroscopic variables (brightness, lifetime, emission spectrum or FRET efficiency) are highly coupled. For the ABN series of constructs, we expected to measure spectroscopic states on a smooth manifold in this parameter space, as has been previously reported by others.^{27,34} To access different sectors of the spectroscopic detection space, this manifold must be shifted by altering the photophysical properties of one or both fluorophores. Changing only sequence and attachment chemistry of the Cy3 donor or by including an additional Cy3, we created three additional label types with different photophysical properties from ABN, shown in Fig. 1b with key differences circled (red dotted). The “skip” oligos, B_{sk}, are modified B strands that lack the unpaired bases opposing Cy3 and Cy5 (compare with Fig. 1a, orange), lowering the lifetime and quantum efficiency of the donor Cy3 as compared to the ABN series ($\tau_{ABsk0} = 1.25$ ns ± 0.03 , green brightness 0.26 ± 0.007 counts $\text{ms}^{-1} \mu\text{W}^{-1}$). The “cap” oligos, A_c, are modified A oligos that carry an additional single-tethered Cy3 at the 5' end, increasing total brightness and lowering net Cy3 lifetime ($\tau_{AcB0} = 1.07$ ns ± 0.03 , green brightness 0.40 ± 0.011 counts $\text{ms}^{-1} \mu\text{W}^{-1}$). The “internal” oligos, B_{in}, incorporate an additional Cy3 between the 3' end of the bridge strand and the 5' end of the B strand, where it can act as an additional donor to increase brightness with near-normal Cy3 lifetime ($\tau_{ABin0} = 1.51$ ns ± 0.03 , green brightness 0.56 ± 0.015 counts $\text{ms}^{-1} \mu\text{W}^{-1}$). (See Supplementary Note S1, Supplementary Table S2, and Supplementary Fig. S1 for additional details, data, and discussion of donor-only photophysics.)

Bulk emission spectra of 15 different ABN constructs are plotted in Fig. 1c, illustrating the expected increase in Cy5 emission with decreasing N. In Fig. 1d, single-exponent fits to the measured lifetime decays of Cy3 for each type of construct are shown as described above, illustrating the effect of local sequence and attachment chemistry on donor lifetime. In total, 41 FRETfluor constructs were synthesized: 15 of ABN, 8 of AB_{sk}N, 9 of A_cBN, and 9 of AB_{in}N. Most, but not all, constructs were found to be uniquely identifiable at the single molecule level; *vide infra*.

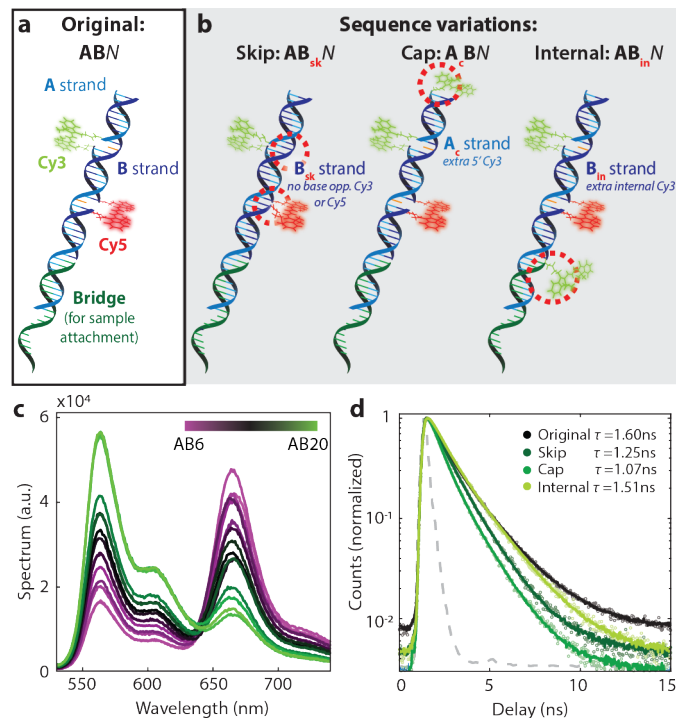


Figure 1. FRETfluor concept and design. a) FRETfluor design for ABN constructs, with a bridge for sequence-specific labeling. b) Oligo sequence and design variations AB_{sk}, A_cB, and AB_{in}, used to create additional unique spectroscopic signatures. Key changes for each construct are highlighted with a dotted red circle. c) Bulk emission spectra of ABN constructs demonstrate that FRET tunes the emission as expected. d) Fluorescence lifetime measurements from single molecules show that Cy3's lifetime depends upon the local DNA sequence (1-exp fits shown).

Detection of FRETfluor labels in the ABEL trap

To spectroscopically characterize the single-molecule emission of each FRETfluor, we employed a custom-built ABEL trap (schematic illustration in Fig. 2a). The ABEL trap applies closed-loop feedback voltages to electrophoretically counteract the effects of Brownian motion in a solution-phase environment. Originally developed by Cohen and Moerner^{48,55} to overcome common technical challenges in single-molecule measurements, the ABEL trap maintains the position of a single molecule conjugate to a point detector for extended time, allowing for an isotropic view under constant illumination without the need for tethers or surfaces. Additional details of ABEL trap operation are available in multiple reviews.^{56–58} Critically, ABEL traps enable detailed multi-parameter spectroscopic observations of single molecules, including brightness, fluorescence lifetime, anisotropy, and emission spectrum.^{49,59,60,51,52,61,22} With the record of applied voltages, trapped particles' observed locations over time can be used to estimate hydrodynamic properties of single particles, including diffusion coefficient and electrophoretic mobility, allowing us to monitor FRETfluor size and charge during trapping.⁵³

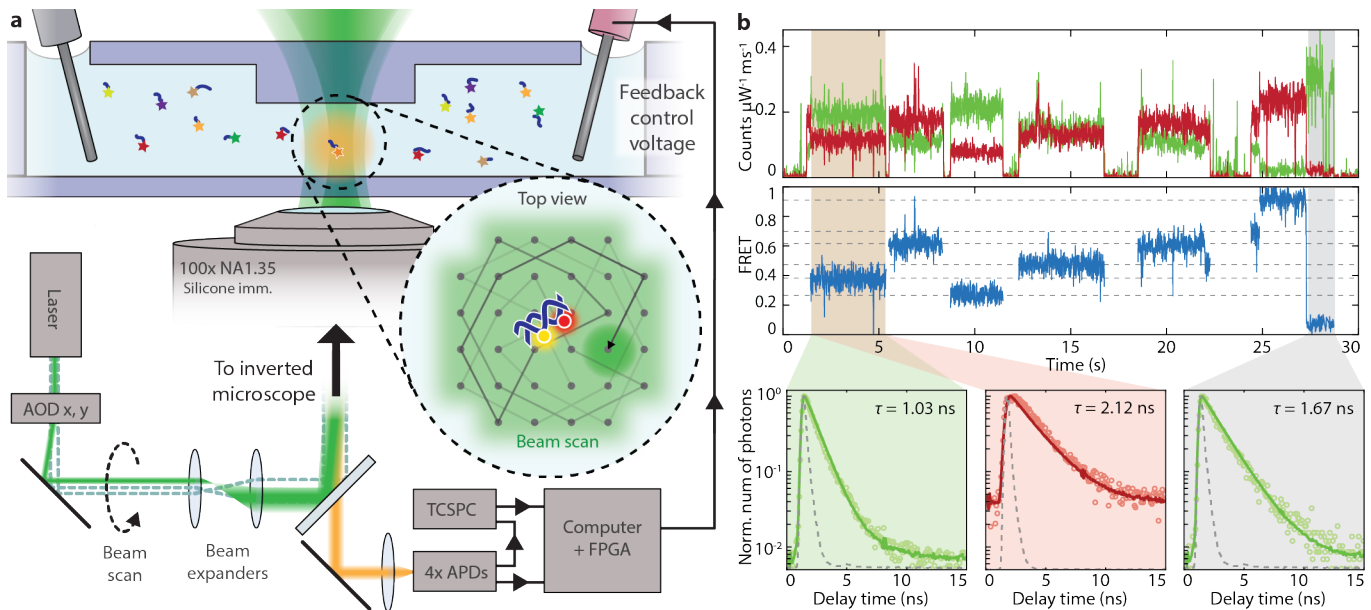


Figure 2. ABEL trap-based detection of FRETfluors in a complex sample. a) Schematic of ABEL trap detection: FRETfluors (blue DNA, colored stars), are detected in a microfluidic cell atop an inverted microscope. 532 nm laser excitation is scanned across the field of view using x and y acousto-optic deflectors (AODs). A FRETfluor in the trapping region fluoresces when it is co-localized with the scanned laser position, enabling closed-loop feedback control over its position via electrodes that apply x and y voltages to electrophoretically move the particle back to trap center. Spectroscopic data is simultaneously acquired. b) Raw ABEL trap data showing signals from 7 different FRETfluors over 30 seconds. *Top*: background-subtracted brightness in red and green channels is observed during trapping. *Middle*: FRET efficiency calculated from red and green brightness. Gray dotted lines indicate expected FRET values for each class of FRETfluor. *Bottom*: Fluorescence lifetime decays for green and red channels during first trapping event (brown \rightarrow green and red backgrounds) vs. when the acceptor is blinking or photobleached (gray background).

In our ABEL trap setup (Fig. 2a), fluorescence from a trapped molecule is collected in red and green emission channels with polarization and lifetime information. During each individual trapping event shown in Fig. 2b, FRET occurs and the FRETfluor identity can be determined by a combination of the

observed parameters. From the lifetime fits, we confirm that the donor lifetime is substantially shortened when energy is being transferred to the Cy5, as expected (Fig. 1b bottom left). At a later time (highlighted in gray), the acceptor Cy5 has either blinked off temporarily, or photobleached, so that we see only the donor Cy3 signal. It is clear that each event exhibits different green and red brightness levels, and different FRET values, (expected FRET values for each type of FRETfluor included for reference, see dotted gray lines). Additional raw ABEL trap data with FRETfluor identity annotated for each trapping event is shown in Supplementary Fig. S2 and discussed in Supplementary Note S2.

Wash-free labeling of specific biomolecular targets

Diverse attachment chemistries, such as small ligands, single-stranded nucleic acids, or peptides, can be conjugated to the end of a FRETfluor DNA oligo. With such attachments, the specificity of FRETfluors to common biomolecular targets can proceed as for other fluorescent labeling strategies, e.g.: antibodies, specific chemical linkers, or sequence complementarity. Here, we demonstrate sequence-specific labeling of nucleic acids including ssDNA and mRNA via sequence complementarity between a single-stranded sequence on the FRETfluor and the desired DNA or RNA target. This is the purpose of the bridge oligo (Fig. 1, green), which hybridizes to the end of the A strand and also to a specific sequence on a target nucleic acid, as illustrated in Fig. 3a. We first verified the FRETfluors' labeling target-specificity by labeling ssDNA oligomers in a bulk electrophoretic mobility shift assay (EMSA; shown in Supplementary Fig. S3). No binding was observed for a bridge sequence lacking complementarity to the ssDNA target ($B_{\text{off-target}}$), while nearly 100% binding was observed with the correct bridge sequence (B_{target}). We also tested binding to mRNA by designing a bridge sequence complementary to a region of eGFP mRNA (996 nt) predicted with high confidence to be part of a loop in the secondary structure.⁶² Bulk EMSAs showed that the off-target bridge sequence could not bind mRNA, while the on-target sequence was hybridized. (See Supplementary Note S3 and Supplementary Fig. S4).

For labeling applications, it is essential to discriminate between on-target binding and free labels. Usually, fluorescence labeling protocols require substantial washing or sample purification, since a correctly bound label cannot be distinguished from an unbound or free tag on the basis of brightness or other spectroscopic properties alone. Here, however, on-target labeling of high molecular-weight samples such as mRNA can be readily confirmed in the ABEL trap via the measured transport properties of the trapped object. Objects with a larger hydrodynamic radius, such as the labelled assemblage, have more charge and will in principle diffuse more slowly than free labels due to larger size, leading to a more tight confinement around the trap's center. The scatter plot in Fig. 3 shows the positional

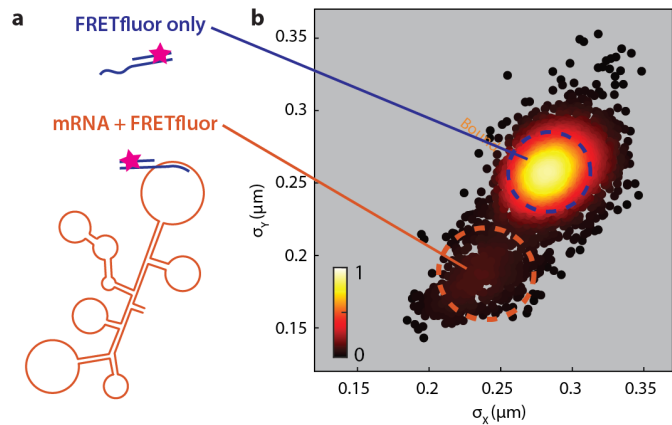


Figure 3. Sequence-specific labeling of mRNA by FRETfluors. a) Illustration of a free FRETfluor tag (upper) and FRETfluor targeting to a specific mRNA (lower). b) Scatter plot of standard deviation of position in x and y for trapped molecules shows two populations. Points are colored according to the local relative scatter plot density.

deviation from trap center in each direction, σ_x and σ_y , for many trapping events. FRETfluors labeling a target mRNA (orange) form a more confined population, with smaller σ_x and σ_y compared to the large population of free labels (blue). The spectroscopic signals observed for labeled mRNA and free FRETfluors were statistically identical (Supplementary Fig. S5).

Multi-parameter characterization of FRETfluor emission

To learn which measured variables captured the most useful information for FRETfluor identification, we collected and aggregated photon-by-photon brightness and lifetime data in four channels (red/green, parallel/perpendicular polarization) from many trapping events. As seen in Fig. 4 for many different constructs, each FRETfluor exhibits tightly-clustered, self-consistent spectroscopic emission. We found that analyzing donor lifetime, FRET efficiency, and red and green channel brightnesses as orthogonal dimensions led to optimal separation and identification of FRETfluor populations.

We tested FRETfluors individually and in various combinations to determine the characteristic emission properties and cluster widths for each construct. Fitted average properties and standard deviations are listed for all 41 constructs in Supplementary Table S3. Fig. 4a shows two different 2-D projections of data from a mixture of nine different AB_N labels. The top projection shows red vs. green brightness (“red-green projection”), and as expected for a series of FRET constructs, these values are approximately inversely correlated. The bottom projection shows the values for single-exponential lifetime fits for the Cy3 donor in the parallel channel vs. FRET efficiency (“lifetime-FRET” projection), which similarly shows an inverse correlation. Nine distinct clusters are clearly evident in each of these projections. Clusters are labeled with the corresponding construct name, as verified by additional experiments using different combinations of constructs, as well as single construct experiments (not shown). The remaining six AB_N constructs were determined to statistically overlap with one or more of the constructs shown here beyond a 2.5% threshold for probability of misclassification of either FRETfluor label (see *Selection of FRETfluor sets for robust classification*), and therefore are not included here (AB7, AB9, AB13, AB15, AB17, AB19). Data for these clusters is shown in Supplementary Fig. S6.

We characterized all other FRETfluor constructs to learn how changes to the donor photophysics shifted the manifold of FRET states observed in the data. Fig. 4b-d show the clusters for combinations from each of the other construct types. Four of eight AB_{skN} constructs showed unique signals relative to the AB_N constructs and one another (Fig. 4b). A subset of the nine AB_N constructs from Fig. 4a was included in this mixture to verify that the AB_{skN} constructs were indeed distinguishable in a mixture (shown in grayscale). Nine A_cB_N constructs and five AB_{inN} constructs were also readily distinguishable relative to the original AB_N constructs (Fig. 4c and d, respectively). Data for all remaining constructs, which were determined to have substantial overlap with other clusters, are shown in Supplementary Fig. S7 and S8.

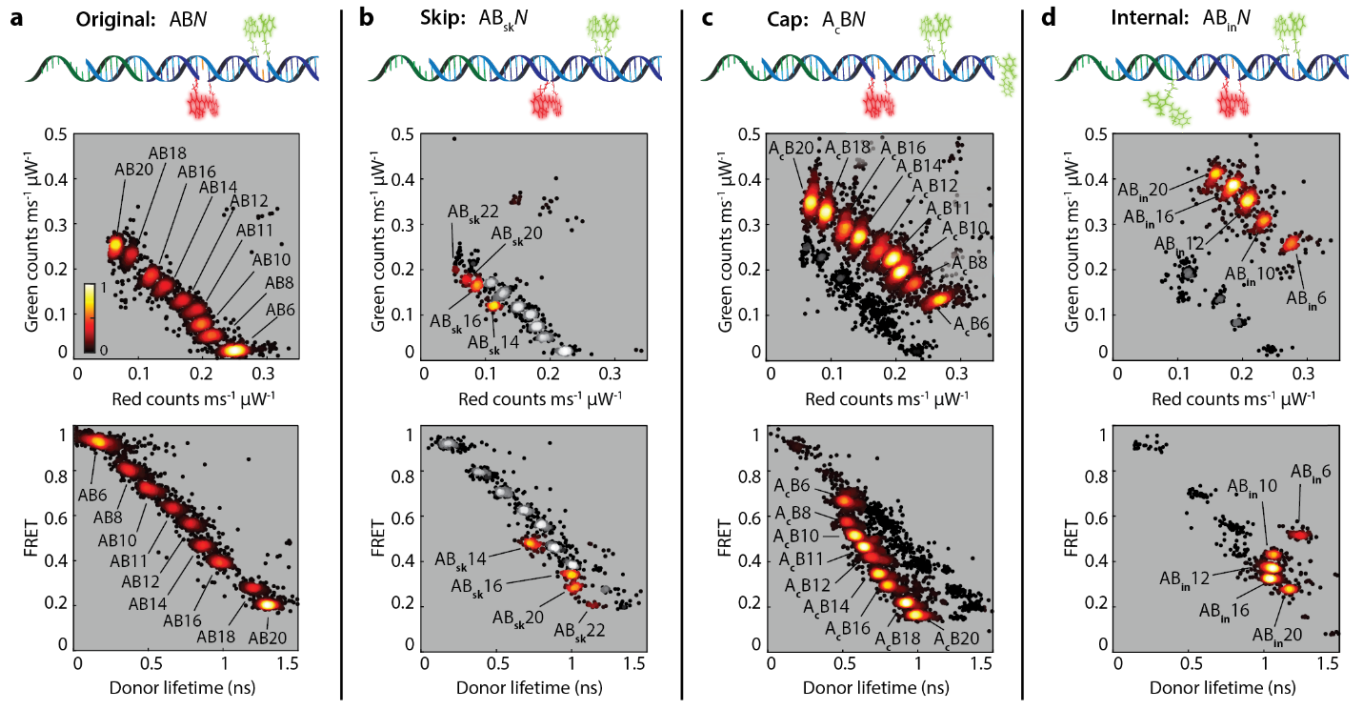


Figure 4. Tuning Cy3 photophysics shifts spectroscopic properties of FRETfluor labels. Red-green and lifetime-FRET projections of data from trapped FRETfluor constructs show clusters in different regions of the measured multi-parameter space. a) A set of 9 ABN constructs show distinct clusters in both red-green (top) and lifetime-FRET (bottom) projections. b) Data for four AB_{sk}N constructs was taken along with nine ABN constructs (grayscale) to verify shifted cluster locations. c) Data for nine A_cBN constructs and d) five AB_{in}N constructs similarly show distinct clusters that are distinguishable from the original ABN construct locations. Throughout: The black-red-yellow heatmap shows relative scatter plot density from low (black) to high (yellow).

Selection of FRETfluor sets for robust classification

We next sought to predict the maximum number of FRETfluors which could be reliably identified in a mixture, which depends on many factors including measurement duration and precision, as well as the set of molecules used for multiplexing and their potential for mis-classification within that set. To this end, we determined the largest set of FRETfluors for which the likelihood of misclassification between any individual pair was below 2.5%. From the pool of 41 FRETfluor constructs tested, we analyzed all possible pairwise combinations to determine which pairs presented higher chances of mutual misclassification. We fitted each cluster from ABEL data as a three-dimensional Gaussian distribution and performed a one-tail integration over the data parameter space to determine the likelihood of each FRETfluor being mis-identified as any other specific FRETfluor.

The matrix in Fig. 5 shows true cluster identity (left) and incorrect cluster identity (bottom), where each square is colored according to the probability of misidentification for that label combination. Any set of FRETfluors can only be used for unambiguous identification in the same sample if all its subset pairs have sufficiently low rates of misidentification. Here, the colorbar is capped at 2.5%, which we chose as a minimum criterion for this work to eliminate unfavorable label combinations. Supplementary Fig. S9 shows the same matrix on a full-scale colorbar (max misidentification probability: ~30% for AB_{sk}10 and AB8). Supplementary Fig. S10 shows the ranked order of pairwise misidentification scores, showing that few (33 of 1640 directional pairs) are above the 2.5% threshold and the likelihood of misclassification for most pairs is vanishingly small. From this analysis we identified a subset of 27 FRETfluors suitable for use in a single mixture (Fig. 5, arrows and Supplementary Table S3, bold) with the misclassification matrix shown in Supplementary Fig. S11.

Multiplexed detection in a complex sample

We then sought to test our ability to distinguish this optimized FRETfluor set experimentally. We combined the complete set of 27 FRETfluors in a dilute (~2 pM total; ~75 fM of each FRETfluor) sample mixture. Fig. 6a shows a red-green projection illustrating clear separation of clusters; these can be further differentiated by inspecting the additional lifetime-FRET projections in Fig. 6b, showing two brightness cuts (above and below a total brightness of 0.37 counts ms⁻¹ μW⁻¹). Fig. 6c shows a 3-D view of the clusters resulting from ABEL trap analysis of this mixture. Each cluster is produced by one FRETfluor label and is colored according to its most likely identity (see *Determination of FRETfluor classification clusters and statistical overlap* for details). Within this three-dimensional red, green brightness and donor lifetime space, each of the 27 FRETfluor populations is easily distinguishable as predicted by Fig. 5 (rotating view of Fig. 6c is provided as Supplementary Video S1). The raw data shown in Supplementary Fig. S2 uses this combination of FRETfluors and is annotated with tag identities. Supplementary Fig. S12 shows the location (oval: 95% confidence interval) for each tag in this mixture, colored according to the construct type.

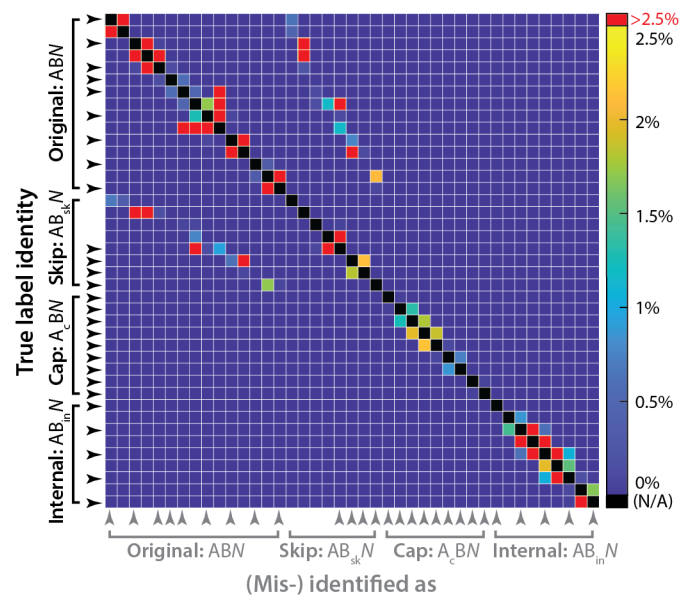


Figure 5. Statistical selection of a near-orthogonal FRETfluor set. One-tailed Gaussian overlap between each pair of clusters was calculated for all 41 constructs. Colorbar represents the probability of misclassification for each pair, and is capped here at 2.5% (red). Self (correct) identification was not considered (black).

Discussion

Our approach to designing FRETfluor labels goes against most conventional wisdom for creating FRET constructs: here we *utilize* the sensitivity of fluorophores to their local environments and attachment chemistries, including local sequence, altering photophysical properties to enhance multiplexing without requiring additional chemical structures. We observed that tuning dye properties allows the characteristic emission properties of entire sets of FRET constructs to be shifted to previously unused sectors of the multi-parameter readout space. Tuning dye properties therefore acts as an additional dimension that expands the design space for engineering constructs with distinctive spectroscopic emission.

We also showed that relatively small changes in dye photophysics are sufficient to produce uniquely identifiable sets of states. The $AB_{sk}N$ constructs are only 15–20% different from the ABN constructs in donor brightness and lifetime, yet generate well-separated states. Critically, for different donor attachment chemistries and sequence contexts, we observed that Cy3-only brightness and lifetime did not change in a perfectly correlated way, indicating that the radiative lifetime must be changing alongside the non-radiative lifetime.⁴⁹ This is particularly useful for FRETfluor design: Supplementary Notes S4 and S5, along with Supplementary Fig. S13, detail additional simulations of FRET on DNA showing that decoupled donor lifetime and brightness lead to nearly orthogonal directional shifts of a FRET curve within the multi-parameter space used in this work. Although not addressed in this work, shifts in the acceptor properties should have similar potential to expand the number of identifiable constructs. We expect that development of more precise control over individual fluorophore properties will only further expand multiplexing possibilities with the approach described here.

Since tuning of dye properties requires altering their local chemical environments, this approach cannot guarantee that the resulting structures will behave completely identically under different conditions (in fact, this is highly unlikely). Nevertheless, it is reasonable to expect that responses to changing sample

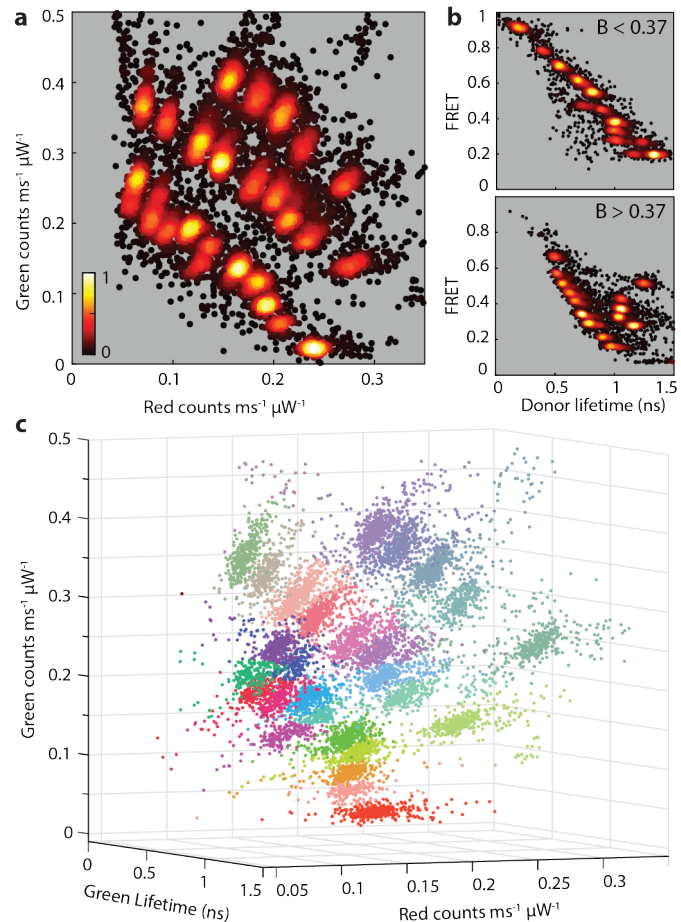


Figure 6. Multiplexed detection of FRETfluors in a complex sample. a) Red-green projection of data. b) Two brightness slices of a lifetime-FRET projection, separated at $B = 0.37$ $\text{counts ms}^{-1} \mu\text{W}^{-1}$ 3-D projection of spectroscopic data; each of 27 FRETfluor labels produces a cluster. Points are colored by cluster membership.

conditions will be more consistent for a fluorophore in two different sequence contexts on DNA than for two chemically different dyes on DNA. The implied advantages of minimal set of chemical components, then, are both practical and technical: Fewer components could lower costs for materials and improve simplicity, and should reduce artefacts from inconsistent chemical properties, thereby improving overall performance.

Additional unique advantages of this approach are conferred by using the ABEL trap for sample readout, in particular its capabilities for extended duration multi-parameter measurements and for estimation of sample transport properties. Here, we were able to multiplex and reliably classify single molecules at ultra-low concentration (tens of femtomolar per species). We did not attempt to optimize throughput in this work; the ABEL trap measures only one molecule at a time, and we did not limit the time spent on each molecule. For higher throughput, a statistically optimal number of photons necessary to correctly identify each species could be determined, and feedback could be turned off after that predetermined time for each detected event, with a small bias voltage to bring new sample into the sensing region. Parallelized microfluidic readout channels and spectroscopic detection could permit additional throughput gains.

Moreover, the approach demonstrated here is in principle cross-compatible with many of the elegant strategies for single-molecule spectroscopic multiplexing that have been proposed by others, including additional excitation lasers, dye ratios, or colors,^{4,3,34} orientational control of dyes to influence polarization,^{27,44} making use of the full distributions available across the multiple detected parameters²³ rather than simplified or averaged values as we show here, as well as with barcoding-types multiplexing strategies such as DNA-PAINT.^{7,12,14} The primary technological advance of our approach is to provide an additional multiplexing dimension, tunable dye photophysics, which is complementary to the multiplexing power of FRET. By multiplexing with constructs created from fewer building blocks, FRETfluors open up new volumes of design space for DNA-FRET-based multiplexing at the single-molecule level.

Methods

DNA oligo samples and preparation

All oligos were purchased with fluorophores from IDT and purified by high-performance liquid chromatography. Full sequences for all oligos are given in Supplementary Table S1. Most oligos include either /iCy3/ or /iCy5/ internal modifications (Cy3 and Cy5 are non-sulfonated). The labeling efficiencies of each strand were 70%-90% by absorption measurements. Double-stranded DNA constructs were annealed by mixing the complementary strands at 5 μ M concentration in TE buffer (pH 8.0), heating to 90 °C for 2 minutes, and slowly cooled down to 25°C with steps of 0.5°C per 20 seconds. DNA samples were stored at 4°C prior to use. Bulk fluorescence emission was characterized with Fluorolog®-3 with FluorEssence™ in shared facilities at the University of Chicago. Bulk fluorescence lifetime measurements for Cy3 were taken with a ChronosBH with magic angle detection and confirmed via bulk measurements on the ABEL setup. For bulk characterization, samples were excited with a 520 nm laser to avoid direct excitation of the acceptor.

Single-molecule characterization in the ABEL trap

A custom Anti-Brownian ELectrokinetic (ABEL) trap was constructed after Ref. 52, incorporating excitation with a pulsed (60MHz) supercontinuum laser (Leukos ROCK 400-4) paired with an AOTF

(Leukos TANGO VIS) to output 532 nm excitation light. The excitation spot was steered in the sample plane using two AODs (MT110-B50A1.5-VIS) arranged orthogonally and driven by a direct digital synthesizer (DDSPA2X-D8b15b-34). Fluorescent photons are split into red and green channels using a dichroic filter (Chroma T610lpxr). Each channel is then split into s and p-polarized light using a polarizing beam splitter (Thorlabs) and focused onto separate APDs (Excelitas SPCM-AQRH-14-ND, four total). For each detected photon, a TCSPC (Picoquant Multiharp 150) records the time and the color and polarization channel in which it arrived.

APD signals are also sent to an FPGA (NI PCIe-78656) which controls the ABEL trap. Based on the position of the laser upon the arrival of each fluorescent photon, taking into account a pre-calibrated lag, the position of the fluorescent molecule is estimated via a noise-rejecting Kalman filter.⁵³ XY voltages proportional to the estimated displacement of the trapped particle relative to the center of the trap are passed to a 10x voltage amplifier (Pendulum F10AD). The amplified voltages are applied to the microfluidic sample cell via platinum electrodes which sit in four reservoirs at the cardinal points of the microfluidic cell.

Immediately prior to measurement, FRETfluors were diluted to a total concentration of between 1-5pM in buffer containing 20 mM HEPES, 3 mM Trolox, and an oxygen scavenging system (~60 nM protocatechuate-3,4-dioxygenase and 2.6 mM protocatechuic acid).

Analysis of ABEL trap data

All data analysis was performed using customized software written in Matlab, after Ref. 52. Briefly, photon arrival times recorded by the Multiharp were used to construct a 10 ms-binned time trace, for which the background levels were identified for each channel using an information-criteria-optimized (AIC) K-means clustering algorithm. Raw photon arrival timestamps were used to identify brightness change points in each channel using the algorithm of Watkins and Yang,⁶³ which were merged into a single list of change points. Data between each pair of change points was assigned to one “level”.

For each level, background-subtracted brightness in all four detection channels was determined and used to calculate a FRET value which was corrected for channel detection efficiency only. Note that here we use both FRET and donor lifetime parameters only for the purpose of separating distinct spectroscopic signals, so that further corrections are not necessary for the purpose of this analysis. For donor lifetimes, we used the green parallel channel only, fitted with a single exponential decay for each level unless otherwise noted. Although 2- and 3-exponential decays provide better fits to the data, for the purpose of this work and given the low photon count in many levels, we observed more robust label classification with 1-exponential fits for lifetime data. Data from levels of duration greater than 150 ms were used for subsequent analysis and can be viewed as individual points in figure scatter plots.

Target labeling

Bridge strand sequences for binding the target ssDNA and with null binding to target ssDNA, the sequence of the ssDNA, and the sequences for the bridge strand for binding and null binding to target mRNA, are given in Supplementary Table S1. We used commercially available EGFP mRNA (CleanCap EGFP mRNA, Trilink BioTechnologies). Electrophoretic mobility shift assay (EMSA) is done by following the existing protocol at room temperature.⁶⁴ The polyacrylamide gel (12%) was run at 200 V in TBE, and the agarose gel (3%) was run at 110 V in 0.5x TAE. Max current was set to 50 mA.

FRETfluor constructs were incubated with the ssDNA target during the annealing process. Incubation with mRNA samples was carried out at room temperature for three hours in labeling buffer (TE pH 8.0) containing RNase inhibitor (1 U/μL, Thermo Scientific RiboLock). After annealing, ABEL trap assay was performed to confirm the mRNA binding.

Determination of FRETfluor classification clusters and statistical overlap

K-means clustering in three dimensions (red and green brightness, donor lifetime) was used for initial classification of events from each data set involving more than one FRETfluor label. The mean and standard deviation in each cluster was determined using a 3-D Gaussian fit without covariance to the cluster after rejecting all outliers ($>3\sigma$ from initial cluster mean). Means and standard deviations from the same FRETfluors across different data sets collected on different days were compared to verify cluster consistency.

Statistical pairwise overlap of these normalized 3-D Gaussians (green brightness, red brightness, green lifetime) was used to calculate the probability of pairwise misclassification, defined as the summed probability in the overlapping tails of each pair of distributions.

References

1. Livet, J. *et al.* Transgenic strategies for combinatorial expression of fluorescent proteins in the nervous system. *Nature* **450**, 56–62 (2007).
2. Nguyen, H. Q. *et al.* Programmable Microfluidic Synthesis of Over One Thousand Uniquely Identifiable Spectral Codes. *Advanced Optical Materials* **5**, 1600548 (2017).
3. Ma, H. *et al.* Multiplexed labeling of genomic loci with dCas9 and engineered sgRNAs using CRISPRainbow. *Nat Biotechnol* **34**, 528–530 (2016).
4. Yim, S. W. *et al.* Four-Color Alternating-Laser Excitation Single-Molecule Fluorescence Spectroscopy for Next-Generation Biodetection Assays. *Clinical Chemistry* **58**, 707–716 (2012).
5. *Principles of Fluorescence Spectroscopy*. (Springer US, 2006). doi:10.1007/978-0-387-46312-4.
6. Chen, K. H., Boettiger, A. N., Moffitt, J. R., Wang, S. & Zhuang, X. Spatially resolved, highly multiplexed RNA profiling in single cells. *Science* **348**, aaa6090 (2015).
7. Jungmann, R. *et al.* Multiplexed 3D cellular super-resolution imaging with DNA-PAINT and Exchange-PAINT. *Nat Methods* **11**, 313–318 (2014).
8. Strauss, S. & Jungmann, R. Up to 100-fold speed-up and multiplexing in optimized DNA-PAINT. *Nat Methods* **17**, 789–791 (2020).
9. Lin, C. *et al.* Submicrometre geometrically encoded fluorescent barcodes self-assembled from DNA. *Nature Chem* **4**, 832–839 (2012).
10. Geiss, G. K. *et al.* Direct multiplexed measurement of gene expression with color-coded probe pairs. *Nat Biotechnol* **26**, 317–325 (2008).
11. Lubeck, E. & Cai, L. Single-cell systems biology by super-resolution imaging and combinatorial labeling. *Nat Methods* **9**, 743–748 (2012).
12. Schnitzbauer, J., Strauss, M. T., Schlichterle, T., Schueder, F. & Jungmann, R. Super-resolution microscopy with DNA-PAINT. *Nat Protoc* **12**, 1198–1228 (2017).
13. Levsky, J. M., Shenoy, S. M., Pezo, R. C. & Singer, R. H. Single-Cell Gene Expression Profiling. *Science* **297**, 836–840 (2002).
14. Wade, O. K. *et al.* 124-Color Super-resolution Imaging by Engineering DNA-PAINT Blinking Kinetics. *Nano Lett.* **19**, 2641–2646 (2019).

15. Makasheva, K. *et al.* Multiplexed Single-Molecule Experiments Reveal Nucleosome Invasion Dynamics of the Cas9 Genome Editor. *J. Am. Chem. Soc.* **143**, 16313–16319 (2021).
16. Shah, S., Dubey, A. K. & Reif, J. Improved Optical Multiplexing with Temporal DNA Barcodes. *ACS Synth. Biol.* **8**, 1100–1111 (2019).
17. Margittai, M. *et al.* Single-molecule fluorescence resonance energy transfer reveals a dynamic equilibrium between closed and open conformations of syntaxin 1. *Proc. Natl. Acad. Sci. U.S.A.* **100**, 15516–15521 (2003).
18. Heilemann, M. *et al.* High-Resolution Colocalization of Single Dye Molecules by Fluorescence Lifetime Imaging Microscopy. *Anal. Chem.* **74**, 3511–3517 (2002).
19. Widengren, J. *et al.* Single-Molecule Detection and Identification of Multiple Species by Multiparameter Fluorescence Detection. *Anal. Chem.* **78**, 2039–2050 (2006).
20. Digman, M. A., Caiolfa, V. R., Zamai, M. & Gratton, E. The Phasor Approach to Fluorescence Lifetime Imaging Analysis. *Biophysical Journal* **94**, L14–L16 (2008).
21. Zhang, Z., Kenny, S. J., Hauser, M., Li, W. & Xu, K. Ultrahigh-throughput single-molecule spectroscopy and spectrally resolved super-resolution microscopy. *Nat Methods* **12**, 935–938 (2015).
22. Squires, A. H. *et al.* Single-molecule trapping and spectroscopy reveals photophysical heterogeneity of phycobilisomes quenched by Orange Carotenoid Protein. *Nature communications* **10**, 1–12 (2019).
23. Niehörster, T. *et al.* Multi-target spectrally resolved fluorescence lifetime imaging microscopy. *Nat Methods* **13**, 257–262 (2016).
24. Barth, A., Voith Von Voithenberg, L. & Lamb, D. C. Quantitative Single-Molecule Three-Color Förster Resonance Energy Transfer by Photon Distribution Analysis. *J. Phys. Chem. B* **123**, 6901–6916 (2019).
25. Sando, S., Abe, H. & Kool, E. T. Quenched Auto-Ligating DNAs: Multicolor Identification of Nucleic Acids at Single Nucleotide Resolution. *J. Am. Chem. Soc.* **126**, 1081–1087 (2004).
26. Kaur, A., Ellison, M. & Dhakal, S. MASH-FRET: A Simplified Approach for Single-Molecule Multiplexing Using FRET. *Anal. Chem.* **93**, 8856–8863 (2021).
27. Iqbal, A. *et al.* Orientation dependence in fluorescent energy transfer between Cy3 and Cy5 terminally attached to double-stranded nucleic acids. *Proc. Natl. Acad. Sci. U.S.A.* **105**, 11176–11181 (2008).
28. *FRET – Förster Resonance Energy Transfer*. (Wiley, 2013). doi:10.1002/9783527656028.
29. Hellenkamp, B. *et al.* Precision and accuracy of single-molecule FRET measurements—a multi-laboratory benchmark study. *Nat Methods* **15**, 669–676 (2018).
30. Woźniak, A. K., Schröder, G. F., Grubmüller, H., Seidel, C. A. M. & Oesterhelt, F. Single-molecule FRET measures bends and kinks in DNA. *Proc. Natl. Acad. Sci. U.S.A.* **105**, 18337–18342 (2008).
31. Nicoli, F. *et al.* Directional Photonic Wire Mediated by Homo-Förster Resonance Energy Transfer on a DNA Origami Platform. *ACS Nano* **11**, 11264–11272 (2017).
32. Hart, S. M., Gorman, J., Bathe, M. & Schlau-Cohen, G. S. Engineering Exciton Dynamics with Synthetic DNA Scaffolds. *Acc. Chem. Res. acs.accounts.3c00086* (2023) doi:10.1021/acs.accounts.3c00086.
33. Mortensen, K. I., Sung, J., Flyvbjerg, H. & Spudich, J. A. Optimized measurements of separations and angles between intra-molecular fluorescent markers. *Nat Commun* **6**, 8621 (2015).
34. Wilson, H. & Wang, Q. ABEL-FRET: tether-free single-molecule FRET with hydrodynamic profiling. *Nat Methods* **18**, 816–820 (2021).
35. Seidel, C. A. M., Schulz, A. & Sauer, M. H. M. Nucleobase-Specific Quenching of Fluorescent Dyes. 1. Nucleobase One-Electron Redox Potentials and Their Correlation with Static and Dynamic Quenching Efficiencies. *J. Phys. Chem.* **100**, 5541–5553 (1996).
36. Levitus, M. & Ranjit, S. Cyanine dyes in biophysical research: the photophysics of polymethine fluorescent dyes in biomolecular environments. *Quart. Rev. Biophys.* **44**, 123–151 (2011).

37. Kretschy, N., Sack, M. & Somoza, M. M. Sequence-Dependent Fluorescence of Cy3- and Cy5-Labeled Double-Stranded DNA. *Bioconjugate Chem.* **27**, 840–848 (2016).

38. Stennett, E. M. S., Ma, N., van der Vaart, A. & Levitus, M. Photophysical and Dynamical Properties of Doubly Linked Cy3–DNA Constructs. *J. Phys. Chem. B* **118**, 152–163 (2014).

39. Agbavwe, C. & Somoza, M. M. Sequence-Dependent Fluorescence of Cyanine Dyes on Microarrays. *PLoS ONE* **6**, e22177 (2011).

40. Harvey, B. J., Perez, C. & Levitus, M. DNA sequence-dependent enhancement of Cy3 fluorescence. *Photochem Photobiol Sci* **8**, 1105–1110 (2009).

41. Iqbal, A., Wang, L., Thompson, K. C., Lilley, D. M. J. & Norman, D. G. The Structure of Cyanine 5 Terminally Attached to Double-Stranded DNA: Implications for FRET Studies. *Biochemistry* **47**, 7857–7862 (2008).

42. Urnavicius, L., McPhee, S. A., Lilley, D. M. J. & Norman, D. G. The Structure of Sulfoindocarbocyanine 3 Terminally Attached to dsDNA via a Long, Flexible Tether. *Biophysical Journal* **102**, 561–568 (2012).

43. Spiriti, J., Binder, J. K., Levitus, M. & Van Der Vaart, A. Cy3-DNA Stacking Interactions Strongly Depend on the Identity of the Terminal Basepair. *Biophysical Journal* **100**, 1049–1057 (2011).

44. Hart, S. M. *et al.* Engineering couplings for exciton transport using synthetic DNA scaffolds. *Chem* **7**, 752–773 (2021).

45. Widengren, J. & Schwille, P. Characterization of Photoinduced Isomerization and Back-Isomerization of the Cyanine Dye Cy5 by Fluorescence Correlation Spectroscopy. *J. Phys. Chem. A* **104**, 6416–6428 (2000).

46. Sanborn, M. E., Connolly, B. K., Gurunathan, K. & Levitus, M. Fluorescence Properties and Photophysics of the Sulfoindocyanine Cy3 Linked Covalently to DNA. *J. Phys. Chem. B* **111**, 11064–11074 (2007).

47. Cunningham, P. D. *et al.* Optical Properties of Vibronically Coupled Cy3 Dimers on DNA Scaffolds. *J. Phys. Chem. B* **122**, 5020–5029 (2018).

48. Cohen, A. E. & Moerner, W. Suppressing Brownian motion of individual biomolecules in solution. *Proceedings of the National Academy of Sciences* **103**, 4362–4365 (2006).

49. Goldsmith, R. H. & Moerner, W. E. Watching conformational- and photodynamics of single fluorescent proteins in solution. *Nature Chem* **2**, 179–186 (2010).

50. Schlau-Cohen, G. S., Wang, Q., Southall, J., Cogdell, R. J. & Moerner, W. E. Single-molecule spectroscopy reveals photosynthetic LH2 complexes switch between emissive states. *Proceedings of the National Academy of Sciences* **110**, 10899–10903 (2013).

51. Wang, Q. & Moerner, W. E. Dissecting pigment architecture of individual photosynthetic antenna complexes in solution. *Proc Natl Acad Sci USA* **112**, 13880–13885 (2015).

52. Squires, A. H. & Moerner, W. Direct single-molecule measurements of phycocyanobilin photophysics in monomeric C-phycocyanin. *Proceedings of the National Academy of Sciences* **114**, 9779–9784 (2017).

53. Wang, Q. & Moerner, W. E. Single-molecule motions enable direct visualization of biomolecular interactions in solution. *Nat Methods* **11**, 555–558 (2014).

54. Lee, W., von Hippel, P. H. & Marcus, A. H. Internally labeled Cy3/Cy5 DNA constructs show greatly enhanced photo-stability in single-molecule FRET experiments. *Nucleic Acids Research* **42**, 5967–5977 (2014).

55. Cohen, A. E. & Moerner, W. Method for trapping and manipulating nanoscale objects in solution. *Applied physics letters* **86**, 093109 (2005).

56. Fields, A. P. & Cohen, A. E. Electrokinetic trapping at the one nanometer limit. *Proceedings of the National Academy of Sciences* **108**, 8937–8942 (2011).

57. Wang, Q., Goldsmith, R. H., Jiang, Y., Bockenhauer, S. D. & Moerner, W. E. Probing Single Biomolecules in Solution Using the Anti-Brownian Electrokinetic (ABEL) Trap. *Acc. Chem. Res.* **45**, 1955–1964 (2012).
58. Squires, A. H., Cohen, A. E. & Moerner, W. E. Anti-Brownian Traps. in *Encyclopedia of Biophysics* (eds. European Biophysical Societies, Roberts, G. & Watts, A.) 1–8 (Springer Berlin Heidelberg, 2018). doi:10.1007/978-3-642-35943-9_486-1.
59. Jiang, Y. *et al.* Sensing cooperativity in ATP hydrolysis for single multisubunit enzymes in solution. *Proc. Natl. Acad. Sci. U.S.A.* **108**, 16962–16967 (2011).
60. Schlau-Cohen, G. S. *et al.* Single-Molecule Identification of Quenched and Unquenched States of LHCII. *J. Phys. Chem. Lett.* **6**, 860–867 (2015).
61. Yang, H.-Y. & Moerner, W. E. Resolving Mixtures in Solution by Single-Molecule Rotational Diffusivity. *Nano Lett.* **18**, 5279–5287 (2018).
62. Hofacker, I. L. Vienna RNA secondary structure server. *Nucleic Acids Research* **31**, 3429–3431 (2003).
63. Watkins, L. P. & Yang, H. Detection of Intensity Change Points in Time-Resolved Single-Molecule Measurements. *J. Phys. Chem. B* **109**, 617–628 (2005).
64. Hellman, L. M. & Fried, M. G. Electrophoretic mobility shift assay (EMSA) for detecting protein–nucleic acid interactions. *Nat Protoc* **2**, 1849–1861 (2007).

Acknowledgment

The authors acknowledge valuable discussions and feedback from: Natalie Tsang, David Pincus, Justin Jureller, Juan de Pablo, and members of the Squires Lab. This work was supported by the Neubauer Family Foundation, as well as NSF QLCI QuBBE grant OMA-2121044 and NSF MRSEC seed funding to A.H.S.

Author contributions

J.C., A.E. and A.H.S conceived and designed constructs and experiments. J.C., A.E., M.R.J., and K.M.L. performed experiments. A.E. and A.H.S. constructed the ABEL trap, and J.C. fabricated microfluidic measurement cells. J.C., A.E., and A.H.S. analyzed data and created figures. A.E.C., J.C., A.E., and A.H.S. worked on simulations. J.C., A.E., and A.H.S. wrote the manuscript. All authors reviewed and edited the manuscript.

Competing interests

None

Materials and correspondence

Correspondence should be directed to asquires@uchicago.edu. The authors declare that the data supporting the findings of this study are available within the paper and its Supplementary Information files. Should any raw data files be needed in another format they are available from the corresponding author upon reasonable request. Oligo sequences for all unique materials created in this work are detailed in Supplementary Table S1 and are commercially available.

Single-molecule fluorescence multiplexing by multi-parameter spectroscopic detection of nanostructured FRET labels

Jiachong Chu^{1*}, Ayesha Ejaz^{2*}, Madeline R. Joseph¹, Aria E. Coraor¹, Kyle M. Lin^{3,4}, and Allison H. Squires^{1,5△}

¹Pritzker School of Molecular Engineering, University of Chicago, IL, USA

²Department of Chemistry, University of Chicago, IL, USA

³Graduate Program in Biophysical Sciences, University of Chicago, Chicago, IL, USA

⁴Medical Scientist Training Program, Pritzker School of Medicine, University of Chicago, Chicago, IL, USA

⁵Institute for Biophysical Dynamics, University of Chicago, Chicago, IL, USA

*Authors contributed equally to this work

△e-mail correspondence: asquires@uchicago.edu

Table of Contents

Table of Contents.....	2
Supplementary Figures	3
Figure S1. Single-molecule brightness and lifetime data for donor-only constructs.....	3
Figure S2. Extended raw data trace for ABEL trapping of single tags.....	4
Figure S3. Binding to ssDNA.....	5
Figure S4. mRNA and DNA binding gel shifts	7
Figure S5. Spectroscopic signal comparison between labeled and unlabeled FRETfluor tags	8
Figure S6. Additional constructs from the ABN series that are not shown in Fig. 4.....	9
Figure S7. Additional constructs from the AB _{sk} N series that are not shown in Fig. 4.....	10
Figure S8. Additional constructs from the AB _{in} N series that are not shown in Fig. 4.....	11
Figure S9. The detail of the pairwise distribution analysis	12
Figure S10. Pairwise misidentification distributions.....	13
Figure S11. Statistical selection of a near-orthogonal FRETfluor set.....	14
Figure S12. Plots are displayed for the gaussian distribution of 27 tags	15
Figure S13. Simple geometrical model for FRET on DNA.....	16
Supplementary tables.....	17
Supplementary Table S1: DNA oligomer sequences for FRETfluors	17
Supplementary Table S2: Lifetime fitting of donor-only constructs.....	18
Supplementary Table S3: FRETfluor cluster locations	19
Supplementary Notes	21
Supplementary Note S1: Sequence- and attachment-dependent photophysics of Cy3	21
Supplementary Note S2: Raw trapping events.....	22
Supplementary Note S3: Sequence of the mRNA with binding site.....	22
Supplementary Note S4: Simulation of energy transfer between Cy3 and Cy5 on dsDNA.....	23
Supplementary Note S5: Effect of changing donor photophysical properties on FRET	25
References	27

Supplementary Figures

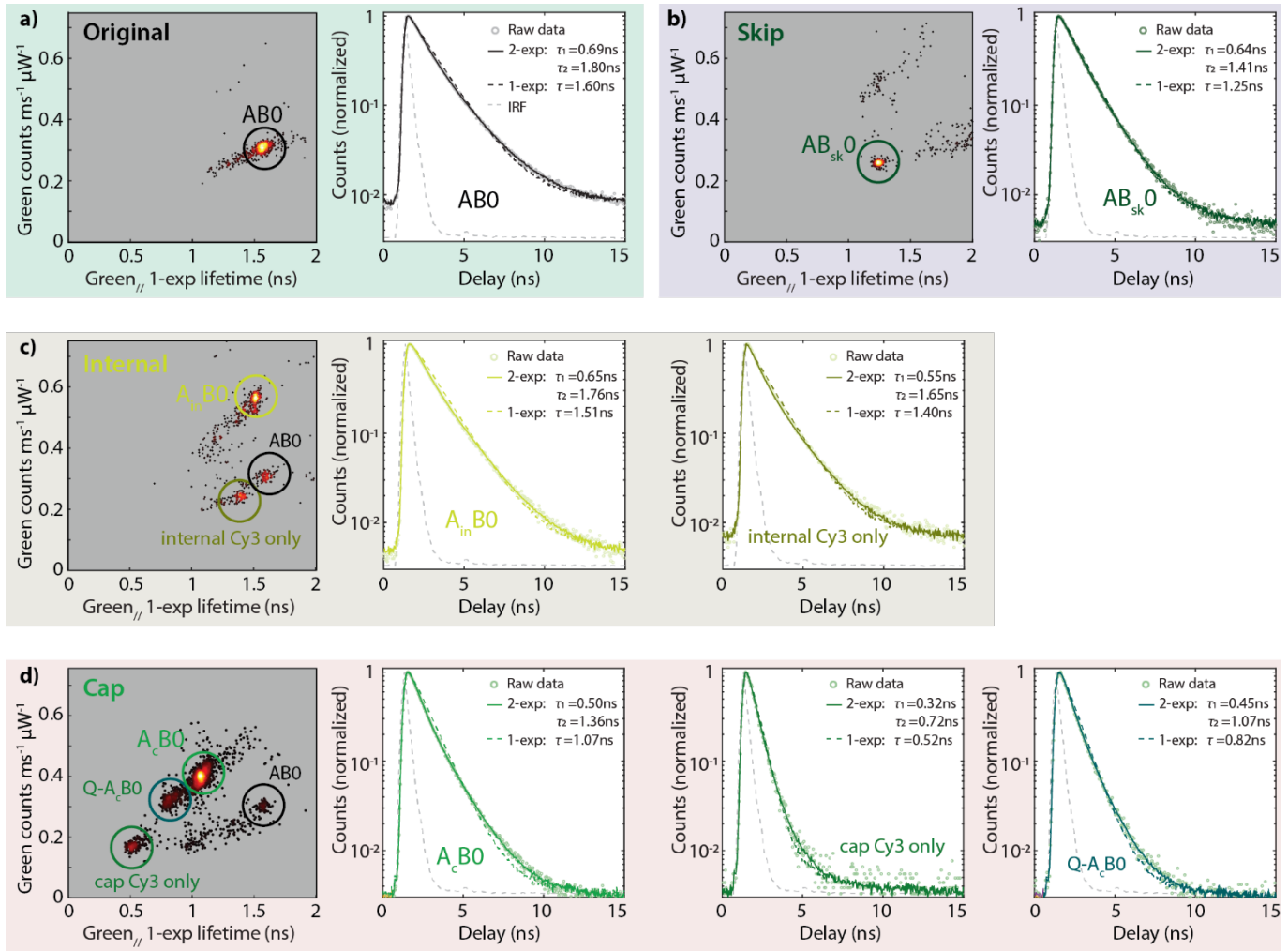


Figure S1. Single-molecule brightness and lifetime data for donor-only constructs. a) Construct AB0 shows one cluster. b) Construct AB_{sk}0 also shows just one population with a slightly shorter lifetime and dimmer brightness. Note that the changes in brightness and lifetime are not proportional to one another. c) Construct A_{in}BO shows three populations: the original AB0 population, a population for the internal Cy3 label, and the majority population when both Cy3s are on. d) The A_cBO constructs should multiple states, of which the brightest population has both Cy3s on (as verified by allowed transitions into and out of this state). The AB0 population is unchanged. The cap-Cy3-only population can be deduced to be the dim, short-lifetime population. The fourth population is unknown. In all cases, the 2-component lifetime fits are superior, but the 1-component lifetime fits adequately represent the weighted average of the better fits.

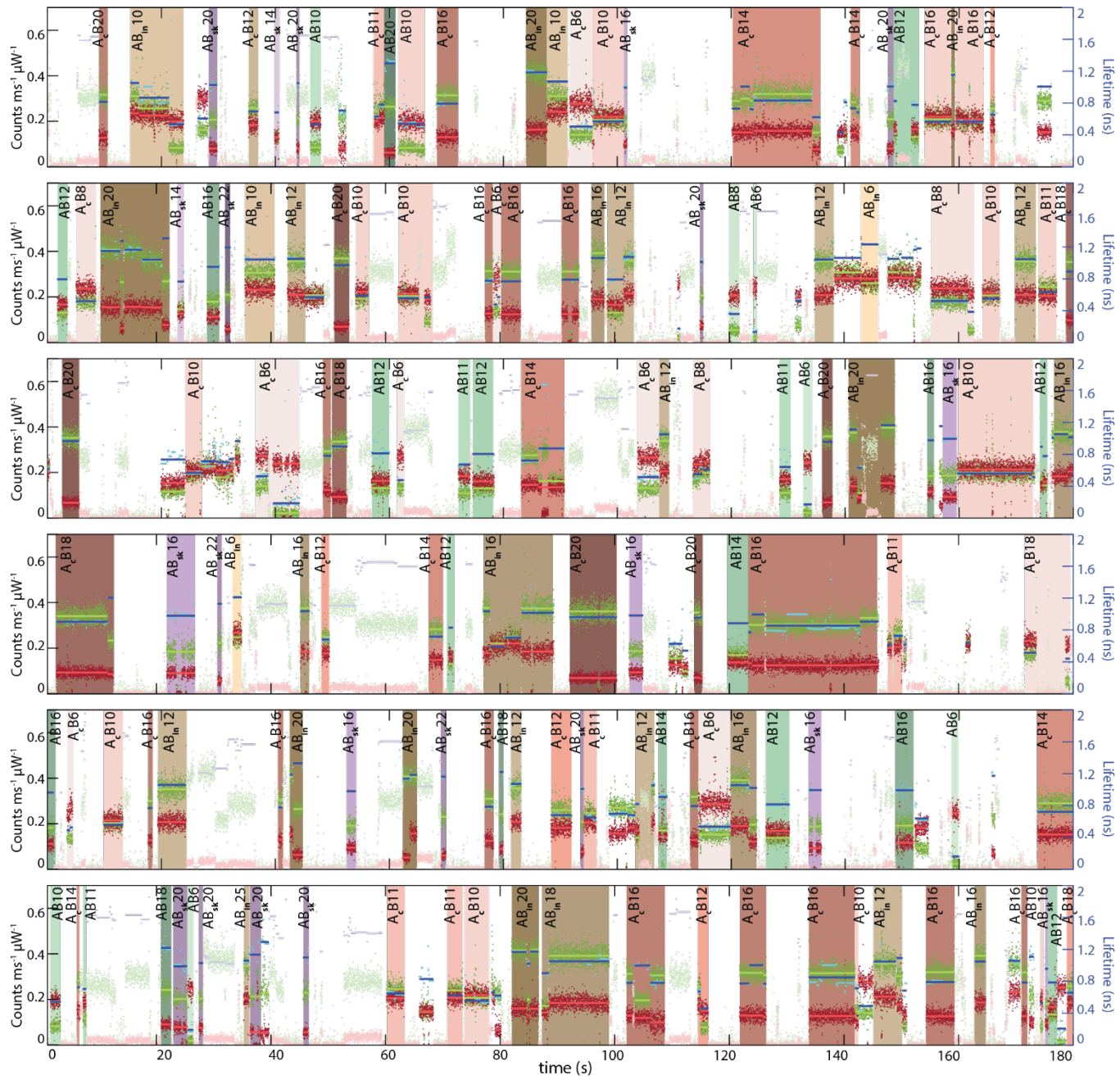


Figure S2. Extended raw data trace for ABEL trapping of single tags. Raw trapping data is shown for green brightness, red brightness, and green channel lifetime for 27 unique FRETfluor tags over a representative 18-minute data set. After events were filtered out when the red channel brightness is lower than $0.5 \text{ counts ms}^{-1} \mu\text{W}^{-1}$, the rest of the events were identified according to the most likely cluster identity from Supplementary Table S3, with a limit of 1 standard deviation from the mean. Most unclassified (dim) events are excluded because they are donor-only. Highlight colors and FRETfluor labels correspond to the populations illustrated in Supplementary Fig. S12.

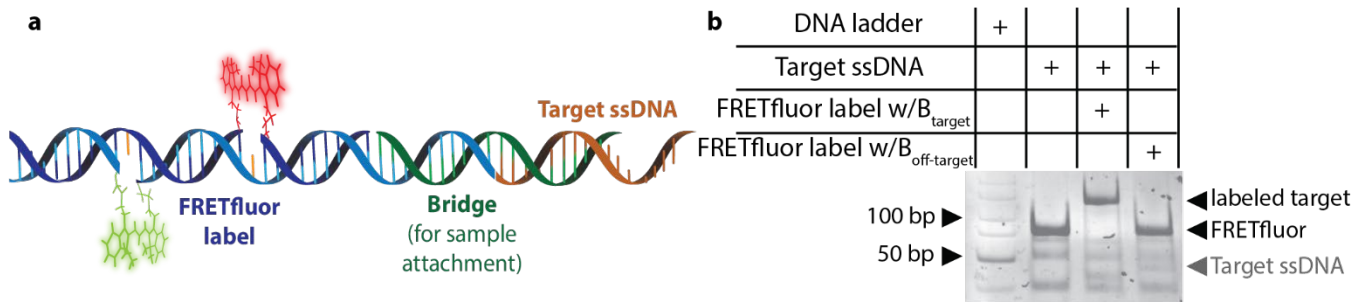


Figure S3. Binding to ssDNA. a) Illustration of the FRETfluor construct hybridized to a ssDNA target sequence (blue: FRETfluor tag, green: labeling bridge, orange: target DNA). b) EMSA showing a mobility shift for on-target binding to a 55bp ssDNA (lane 3) as compared to free label (lane 2), but no shift for an off-target bridge sequence (lane 4).

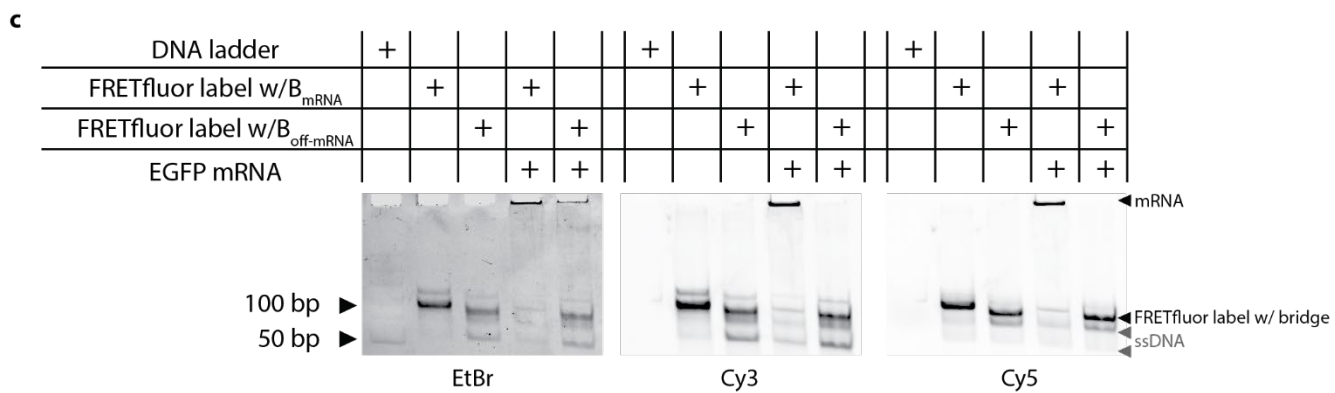
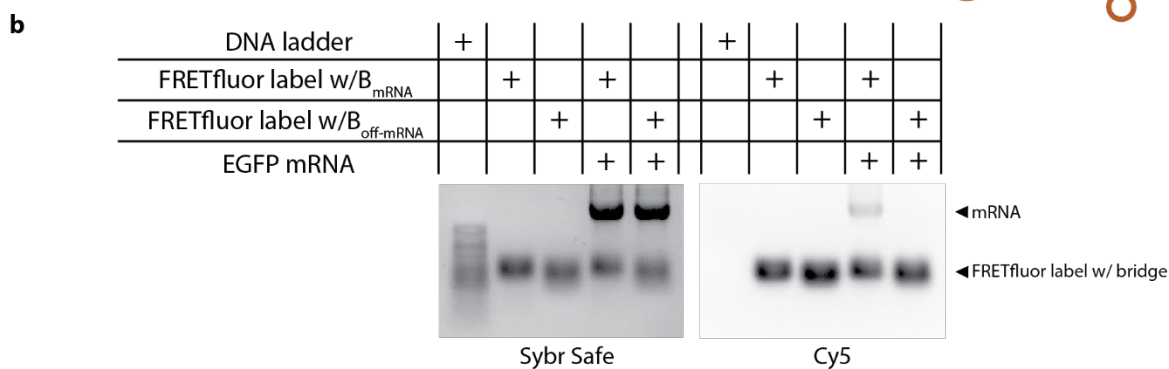
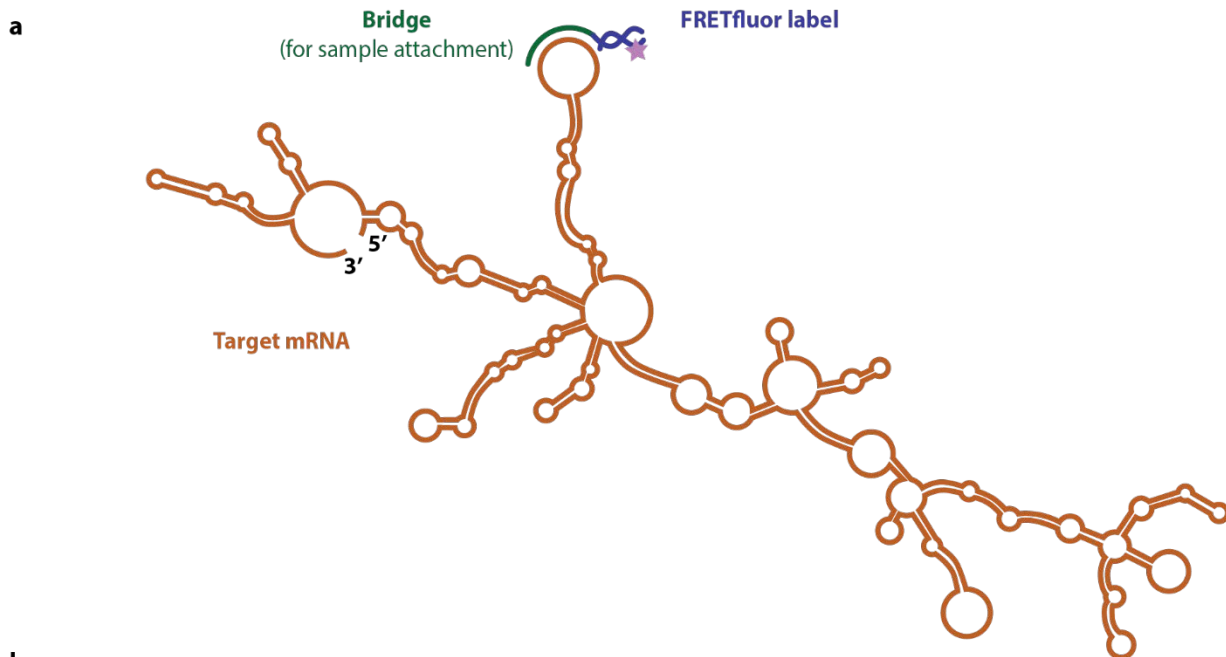


Figure S4. mRNA and DNA binding gel shifts. a) Illustration of a FRETfluor label (blue) attached to a predicted hairpin loop of the eGFP mRNA through a labeling bridge (green). b) Electrophoretic mobility shift assay (EMSA) on an agarose gel showing a mobility shift for on target binding to a EGFP mRNA as compared to free label (lanes 2 and 3), but no shift for an mismatched labeling bridge. The gel was scanned in two different excitation channels: Trans UV for SyberSafe and Cy5 excitation channel. c) EMSA on a 12% polyacrylamide gel reveals more detail about binding specificity. The gel was scanned in three different excitation channels: Trans UV for EtBr, Cy3 excitation channel and Cy5 excitation channel. Due to the high gel percentage, all mRNA is trapped the loading well because it is too big to be pushed down, but the correct FRETfluor is clearly bound in lane 4, and not bound at all with the mismatched bridge sequence in lane 5.

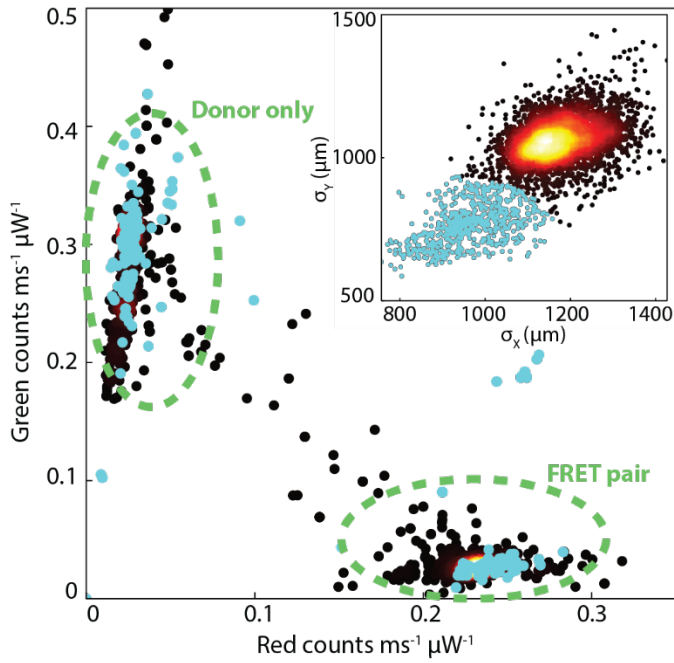


Figure S5. Spectroscopic signal comparison between labeled and unlabeled FRETfluor tags. Cyan points show the spectroscopic signal from tags in the FRETfluor+mRNA correctly labeled population, which has a lower σ_x and σ_y . The signal from this population is overlapping with those that are not labeled on the target mRNA. There are two clusters of spectroscopic signal on the red counts vs green counts plot. The one that has higher green counts but is lower in the red channel represents the donor-only signal, and the one that has lower green counts but is high in the red channel represents the energy transfer between the donor and acceptor. The labeled FRETfluor tags are aligned with both of the signal clusters.

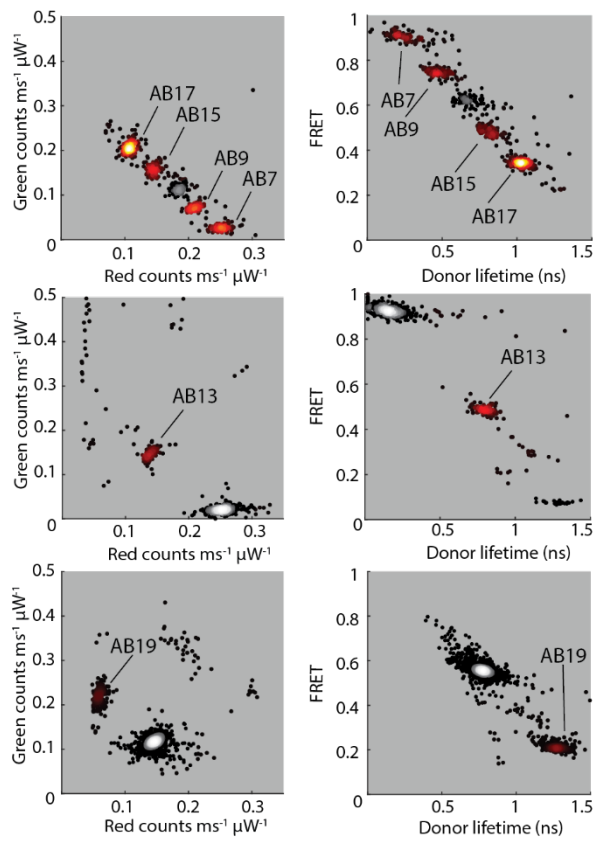


Figure S6. Additional constructs from the ABN series that are not shown in Fig. 4.: Red-green and lifetime-FRET projections of data from trapped FRETfluors with design variations show clusters in different regions of the parameter space.

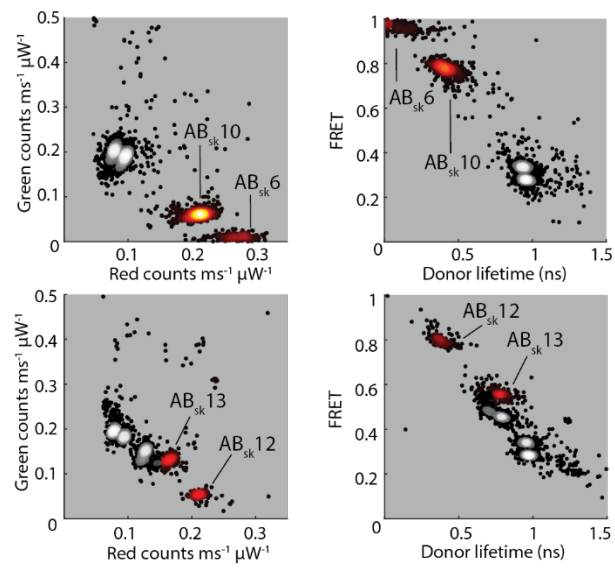


Figure S7. Additional constructs from the $AB_{sk}N$ series that are not shown in Fig. 4.: Red-green and lifetime-FRET projections of data from trapped FRETfluors with design variations show clusters in different regions of the parameter space.

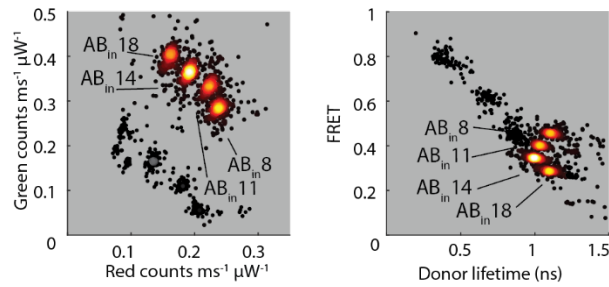


Figure S8. Additional constructs from the AB_{in}N series that are not shown in Fig. 4.: Red-green and lifetime-FRET projections of data from trapped FRETfluors with design variations show clusters in different regions of the parameter space.

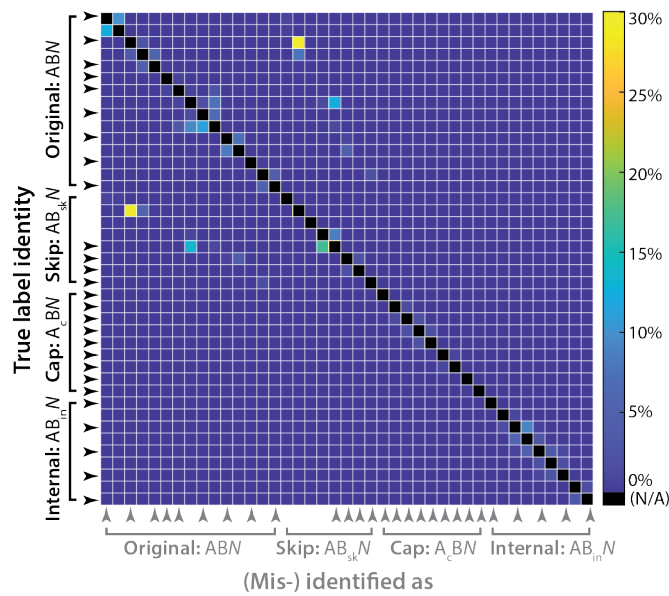


Figure S9. The detail of the pairwise distribution analysis. Statistical selection of a near-orthogonal FRETfluor set. One-tailed Gaussian overlap between each pair of clusters was calculated for all 41 constructs. The color bar cutoff is 30%.

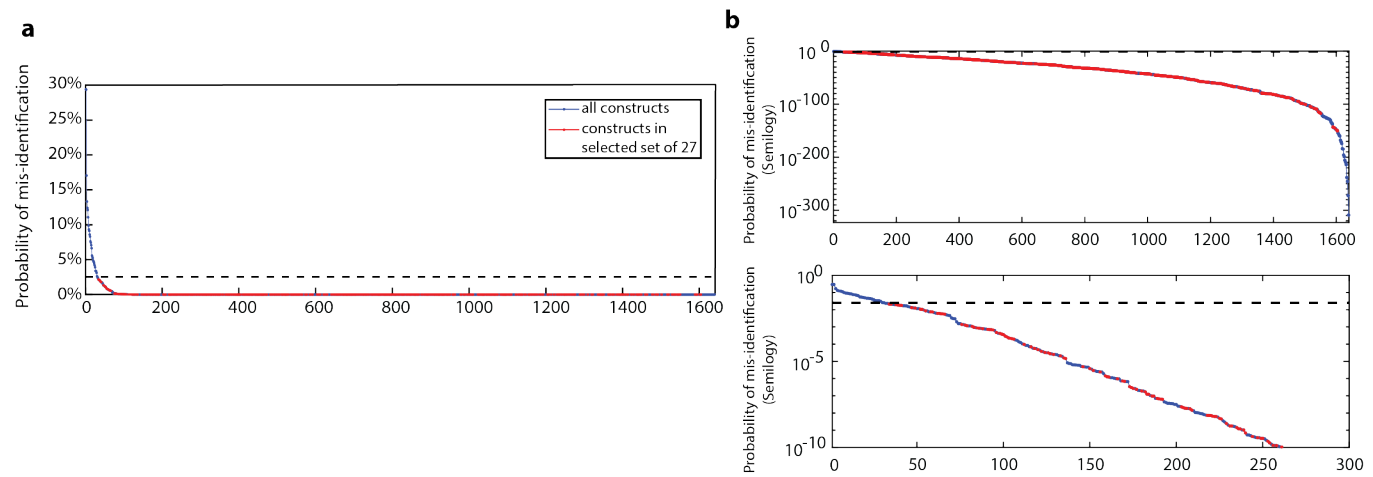


Figure S10. Pairwise misidentification distributions. a) The ranked probabilities of pairwise misidentification for all possible FRETfluor pairs. b) Same data, y-axis shown on a log scale. Top panel is the full plot, bottom is zoomed in to show detail for higher probabilities.

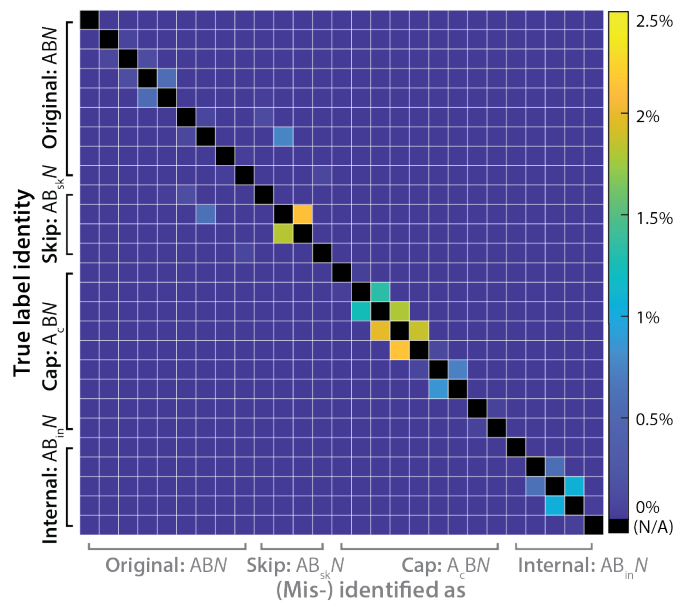


Figure S11. Statistical selection of a near-orthogonal FRETfluor set. One-tailed Gaussian overlap between each pair of clusters was calculated for the 27 selected constructs. The color bar cutoff is 2.5%.

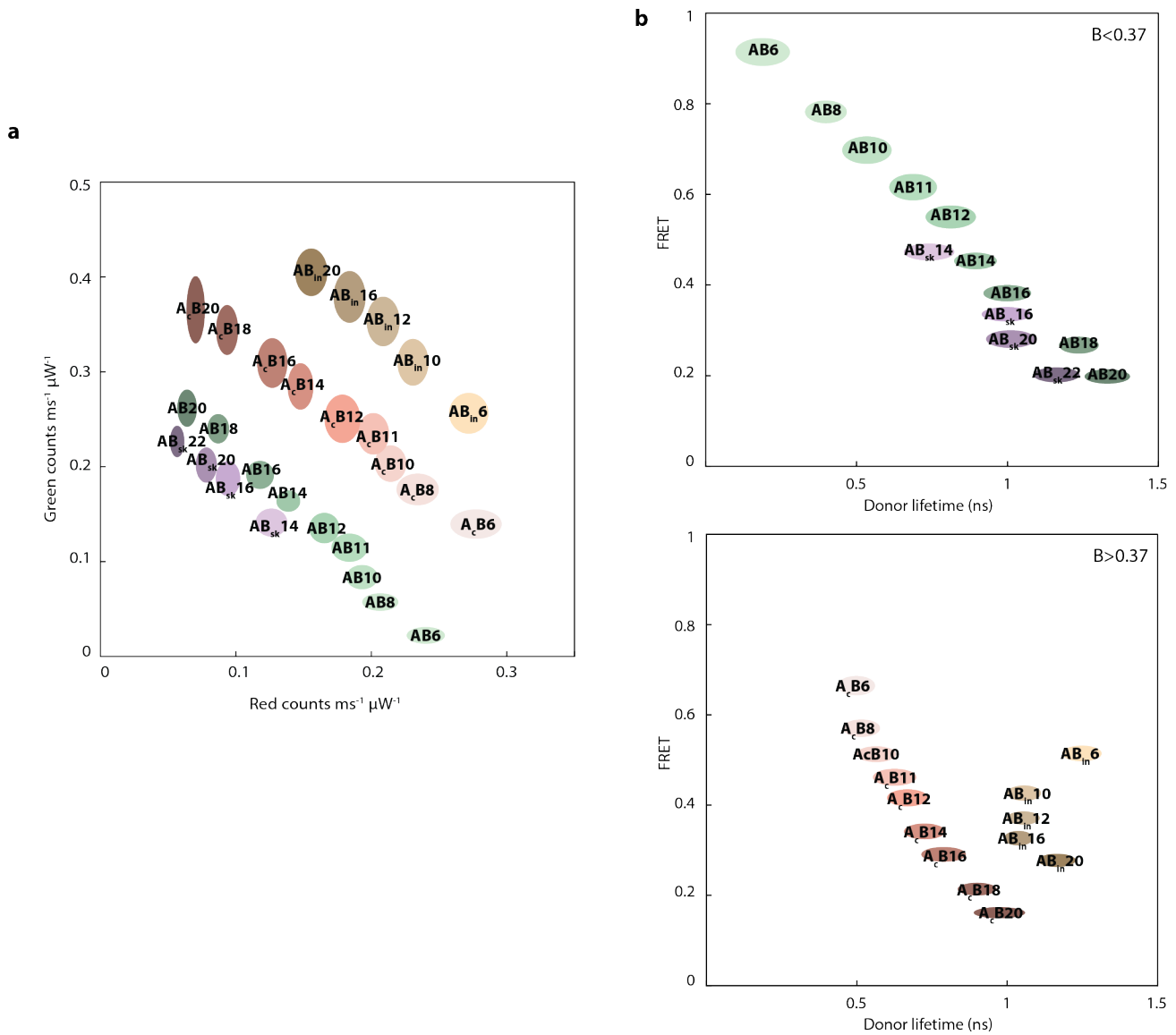


Figure S12. Plots are displayed for the gaussian distribution of 27 tags. a) Red-green projection of data, plotted with the calculated center and 95% confidence interval oval. b) Two brightness slices of lifetime-FRET projection of data, plotted with the calculated center and 95% confidence interval oval.

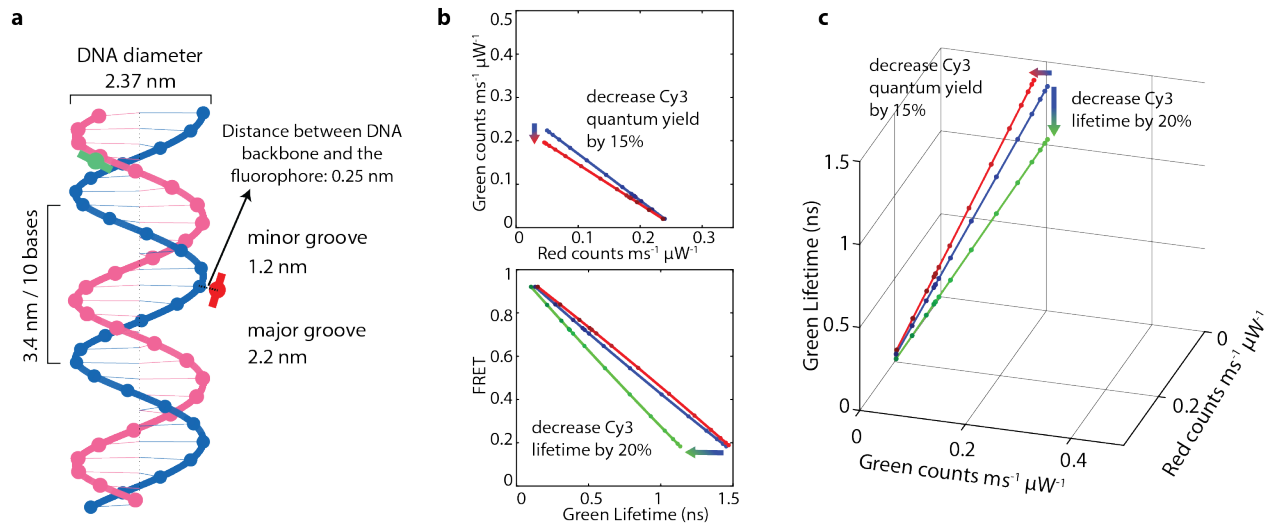


Figure S13. Simple geometrical model for FRET on DNA. a) Cartoon of a rigid DNA double helix with doubly-tethered Cy3 and Cy5 incorporated into the backbone (shown: spacing similar to AB7). b) The calculated spectroscopic signal when the Cy3 quantum yield is reduced by 15% (red) as compared to the original quantum yield (blue). The green line represents a Cy3 lifetime reduced by 20%. c) A three-dimensional view of the model results shows that decoupled changes to quantum yield and lifetime move the FRET curve in nearly orthogonal directions in the detection parameter space.

Supplementary tables

Supplementary Table S1: DNA oligomer sequences for FRETfluors

Ashort	5'	GAT GAT GTC ATC GAC /iCy3 /GCG CGA TAT TCC TAC TTA TGG CGG CTC TTC CCA G	3'
A	5'	GAT GAT GTC ATC GAC /iCy3 /GCG CGA TAT TCC TAC TTA TGG CGG CTC TTC CCA GCG CTA ATC ACG TTC A	3'
A _c	5'	/5Cy3 /GAT GAT GTC ATC GAC /iCy3 /GCG CGA TAT TCC TAC TTA TGG CGG CTC TTC CCA GCG CTA ATC ACG TTC A	3'
B6	5'	CTG GGA AGA GCC GCC ATA AGT AGG AAT /iCy5 /TCG CGC CGT CGA TGA CAT CAT C	3'
B7	5'	CTG GGA AGA GCC GCC ATA AGT AGG AA /iCy5 /A TCG CGC CGT CGA TGA CAT CAT C	3'
B8	5'	CTG GGA AGA GCC GCC ATA AGT AGG A /iCy5 /TA TCG CGC CGT CGA TGA CAT CAT C	3'
B9	5'	CTG GGA AGA GCC GCC ATA AGT AGG /iCy5 /ATA TCG CGC CGT CGA TGA CAT CAT C	3'
B10	5'	CTG GGA AGA GCC GCC ATA AGT AG /iCy5 / AAT ATC GCG CGT TCG ATG ACA TCA TC	3'
B11	5'	CTG GGA AGA GCC GCC ATA AGT A /iCy5 /G AAT ATC GCG CGT TCG ATG ACA TCA TC	3'
B12	5'	CTG GGA AGA GCC GCC ATA AGT /iCy5 /GG AAT ATC GCG CGT TCG ATG ACA TCA TC	3'
B13	5'	CTG GGA AGA GCC GCC ATA AG /iCy5 / AGG AAT ATC GCG CGT TCG ATG ACA TCA TC	3'
B14	5'	CTG GGA AGA GCC GCC ATA A /iCy5 /T AGG AAT ATC GCG CGT TCG ATG ACA TCA TC	3'
B15	5'	CTG GGA AGA GCC GCC ATA /iCy5 /GT AGG AAT ATC GCG CGT TCG ATG ACA TCA TC	3'
B16	5'	CTG GGA AGA GCC GCC AT /iCy5 / AGT AGG AAT ATC GCG CGT TCG ATG ACA TCA TC	3'
B17	5'	CTG GGA AGA GCC GCC A /iCy5 /A AGT AGG AAT ATC GCG CGT TCG ATG ACA TCA TC	3'
B18	5'	CTG GGA AGA GCC GCC /iCy5 /TA AGT AGG AAT ATC GCG CGT TCG ATG ACA TCA TC	3'
B19	5'	CTG GGA AGA GCC GC /iCy5 / ATA AGT AGG AAT ATC GCG CGT TCG ATG ACA TCA TC	3'
B20	5'	CTG GGA AGA GCC G /iCy5 /C ATA AGT AGG AAT ATC GCG CGT TCG ATG ACA TCA TC	3'
B _{sk6}	5'	CTG GGA AGA GCC GCC ATA AGT AGG AAT A /iCy5 /TC GCG CGT CGA TGA CAT CAT C	3'
B _{sk10}	5'	CTG GGA AGA GCC GCC ATA AGT AGG /iCy5 /AAT ATC GCG CGT CGA TGA CAT CAT C	3'
B _{sk12}	5'	CTG GGA AGA GCC GCC ATA AGT A /iCy5 /GG AAT ATC GCG CGT CGA TGA CAT CAT C	3'
B _{sk13}	5'	CTG GGA AGA GCC GCC ATA AGT /iCy5 /AGG AAT ATC GCG CGT CGA TGA CAT CAT C	3'
B _{sk14}	5'	CTG GGA AGA GCC GCC ATA AG /iCy5 /T AGG AAT ATC GCG CGT CGA TGA CAT CAT C	3'
B _{sk16}	5'	CTG GGA AGA GCC GCC ATA /iCy5 / AGT AGG AAT ATC GCG CGT CGA TGA CAT CAT C	3'
B _{sk20}	5'	CTG GGA AGA GCC GC /iCy5 /C ATA AGT AGG AAT ATC GCG CGT CGA TGA CAT CAT C	3'
B _{sk22}	5'	CTG GGA AGA GCC /iCy5 /GCC ATA AGT AGG AAT ATC GCG CGT CGA TGA CAT CAT C	3'
B _{in}	5'	TGA ACG TGA TTA GCG /3Cy3 /	3'
B _{target}	5'	AAC TGC CTG GTG ATA TGA ACG TGA TTA GCG	3'
B _{off-target}	5'	ATT CCT AAG TCT GAA TGA ACG TGA TTA GCG	3'
target	5'	TAT CAC CAG GCA GTT GAC AGT GTA GCA AGC TGT AAT AGA TGC GAG GGT CCA ATA C	3'
B _{mRNA}	5'	TGT TCT GCT GGT AGT GGT GAA CGT GAT TAG CG	3'
B _{off-RNA}	5'	AAC ACA TAA ATA AAA TGA ACG TGA TTA GCG	3'
B _{biotin}	5'	/5Biosg/TGA ACG TGA TTA GCG	3'

KEY for Supplementary Table S1:

- X:** Base is opposite to Cy3 after annealing
- XX:** No base immediately opposite to Cy3, so the Cy3 will be more exposed to solvent
- X/iCy5/X:** No base immediately opposite to Cy5, so the Cy5 will be more exposed to solvent
- XXX/XXX:** Complementary sequences are shown in the same color
- XXX:** Complementary to the GFP mRNA, also highlighted in gray (see SI Note S5)

Supplementary Table S2: Lifetime fitting of donor-only constructs

Construct (population)	Brightness (counts $\mu\text{s}^{-1} \mu\text{W}^{-1}$)	1-exp Lifetime (ns)	2-exp Lifetimes #1 (% population; ns)		2-exp Lifetimes #2 (% population; ns)	
AB0	0.31 ± 0.012	1.60 ± 0.03	$41\% \pm 4.0\%$	0.69 ± 0.05	$59\% \pm 4.0\%$	1.80 ± 0.03
AB_{sk}0	0.26 ± 0.007	1.25 ± 0.03	$37\% \pm 4.5\%$	0.64 ± 0.07	$63\% \pm 4.5\%$	1.41 ± 0.05
AB_{in}0 (AB_{in}0)	0.56 ± 0.015	1.51 ± 0.03	$44\% \pm 1.1\%$	0.65 ± 0.02	$56\% \pm 1.1\%$	1.76 ± 0.02
(bridge Cy3 only)	0.24 ± 0.010	1.40 ± 0.03	$47\% \pm 4.2\%$	0.55 ± 0.03	$53\% \pm 4.2\%$	1.65 ± 0.04
A_cB0 (A_cB0)	0.40 ± 0.011	1.07 ± 0.03	$59\% \pm 1.4\%$	0.50 ± 0.03	$41\% \pm 1.4\%$	1.36 ± 0.02
(cap Cy3 only)	0.17 ± 0.007	0.52 ± 0.02	$70\% \pm 11\%$	0.32 ± 0.06	$30\% \pm 11\%$	0.72 ± 0.08
(Q-A _c B0)	0.32 ± 0.013	0.82 ± 0.03	$62\% \pm 5\%$	0.45 ± 0.04	$38\% \pm 5\%$	1.07 ± 0.04

Supplementary Table S3: FRETfluor cluster locations

Tag	FRET unitless, [0,1]	Donor Lifetime (ns)	Red Brightness (counts $\mu\text{s}^{-1} \mu\text{W}^{-1}$)	Green Brightness (counts $\mu\text{s}^{-1} \mu\text{W}^{-1}$)
AB6	0.916 \pm 0.016	0.187 \pm 0.045	0.240 \pm 0.007	0.022 \pm 0.004
AB7	0.904 \pm 0.016	0.270 \pm 0.049	0.252 \pm 0.010	0.027 \pm 0.005
AB8	0.783 \pm 0.013	0.398 \pm 0.035	0.207 \pm 0.007	0.057 \pm 0.005
AB9	0.743 \pm 0.012	0.486 \pm 0.050	0.210 \pm 0.008	0.073 \pm 0.006
AB10	0.698 \pm 0.015	0.534 \pm 0.041	0.193 \pm 0.006	0.084 \pm 0.006
AB11	0.616 \pm 0.015	0.687 \pm 0.040	0.184 \pm 0.007	0.115 \pm 0.007
AB12	0.550 \pm 0.013	0.813 \pm 0.042	0.165 \pm 0.006	0.135 \pm 0.008
AB13	0.488 \pm 0.011	0.797 \pm 0.035	0.136 \pm 0.006	0.143 \pm 0.009
AB14	0.453 \pm 0.009	0.895 \pm 0.035	0.138 \pm 0.004	0.167 \pm 0.006
AB15	0.482 \pm 0.017	0.839 \pm 0.042	0.148 \pm 0.007	0.159 \pm 0.010
AB16	0.381 \pm 0.009	1.001 \pm 0.040	0.118 \pm 0.005	0.191 \pm 0.007
AB17	0.342 \pm 0.012	1.034 \pm 0.038	0.107 \pm 0.006	0.207 \pm 0.009
AB18	0.266 \pm 0.009	1.238 \pm 0.033	0.087 \pm 0.004	0.240 \pm 0.008
AB19	0.214 \pm 0.007	1.234 \pm 0.030	0.067 \pm 0.004	0.244 \pm 0.013
AB20	0.197 \pm 0.008	1.333 \pm 0.038	0.064 \pm 0.004	0.262 \pm 0.010
AB _{sk} 6	0.962 \pm 0.012	0.125 \pm 0.047	0.272 \pm 0.010	0.011 \pm 0.003
AB _{sk} 10	0.776 \pm 0.014	0.417 \pm 0.033	0.210 \pm 0.008	0.061 \pm 0.004
AB _{sk} 12	0.551 \pm 0.008	0.676 \pm 0.023	0.149 \pm 0.003	0.121 \pm 0.004
AB _{sk} 13	0.480 \pm 0.009	0.699 \pm 0.025	0.123 \pm 0.004	0.133 \pm 0.004
AB_{sk}14	0.472 \pm 0.009	0.741 \pm 0.042	0.126 \pm 0.006	0.141 \pm 0.007
AB_{sk}16	0.334 \pm 0.008	0.998 \pm 0.042	0.094 \pm 0.005	0.188 \pm 0.009
AB_{sk}20	0.279 \pm 0.010	1.011 \pm 0.041	0.078 \pm 0.004	0.202 \pm 0.009
AB_{sk}22	0.200 \pm 0.008	1.164 \pm 0.038	0.057 \pm 0.003	0.227 \pm 0.008
A_cB6	0.665 \pm 0.011	0.498 \pm 0.031	0.277 \pm 0.009	0.140 \pm 0.008
A_cB8	0.571 \pm 0.010	0.515 \pm 0.031	0.234 \pm 0.008	0.176 \pm 0.008
A_cB10	0.513 \pm 0.009	0.564 \pm 0.033	0.214 \pm 0.006	0.203 \pm 0.010
A_cB11	0.462 \pm 0.009	0.626 \pm 0.036	0.202 \pm 0.006	0.235 \pm 0.011
A_cB12	0.416 \pm 0.009	0.669 \pm 0.034	0.179 \pm 0.007	0.251 \pm 0.013
A_cB14	0.342 \pm 0.009	0.725 \pm 0.034	0.148 \pm 0.005	0.285 \pm 0.012
A_cB16	0.291 \pm 0.008	0.789 \pm 0.037	0.127 \pm 0.006	0.309 \pm 0.013
A_cB18	0.214 \pm 0.007	0.900 \pm 0.032	0.094 \pm 0.004	0.344 \pm 0.013
A_cB20	0.161 \pm 0.006	0.975 \pm 0.043	0.070 \pm 0.003	0.365 \pm 0.018
AB_{in}6	0.515 \pm 0.009	1.249 \pm 0.033	0.272 \pm 0.007	0.256 \pm 0.011
AB _{in} 8	0.457 \pm 0.006	1.132 \pm 0.019	0.239 \pm 0.005	0.284 \pm 0.007
AB_{in}10	0.427 \pm 0.009	1.057 \pm 0.028	0.231 \pm 0.006	0.310 \pm 0.012
AB _{in} 11	0.403 \pm 0.005	1.047 \pm 0.018	0.220 \pm 0.004	0.327 \pm 0.007
AB_{in}12	0.372 \pm 0.007	1.054 \pm 0.027	0.209 \pm 0.006	0.353 \pm 0.013
AB _{in} 14	0.344 \pm 0.005	1.017 \pm 0.019	0.203 \pm 0.004	0.387 \pm 0.008
AB_{in}16	0.327 \pm 0.008	1.038 \pm 0.024	0.184 \pm 0.006	0.379 \pm 0.014

AB_{in}18	0.290 \pm 0.005	1.088 \pm 0.017	0.159 \pm 0.004	0.388 \pm 0.008
AB_{in}20	0.278 \pm 0.007	1.166 \pm 0.031	0.156 \pm 0.006	0.405 \pm 0.013

Supplementary Notes

Supplementary Note S1: Sequence- and attachment-dependent photophysics of Cy3

Physical and chemical properties of the nano-environment of a fluorophore, and in particular the resulting dielectric environment, strongly influence fluorophore photophysics. Different solvents, substrates, and attachment chemistries therefore can alter observed photophysical properties from their baseline values; conversely, small modifications to the local environment can be used to intentionally alter these properties, as we have done in this work. Traditionally, the brightness or quantum yield Φ of a fluorophore is expected to change proportionally with the observed lifetime τ , since

$$\tau = \frac{1}{k_r + k_{nr}} \quad (1)$$

and

$$\Phi = \frac{k_r}{k_r + k_{nr}} \quad (2)$$

and the native radiative rate k_r of a fluorophore is assumed to be constant while only k_{nr} changes. However, if the dielectric environment of the fluorophore changes due to changing exposure to solvent or to changes in the chemical surroundings, k_r can also change, decoupling τ and Φ .¹

We measured the brightness and fluorescence lifetime of Cy3 alone for each type of construct used in this work. In all naming conventions used here, a “0” denotes the lack of a Cy5 dye on the B strand. Supplementary Figure S1 shows aggregated single-molecule data for Cy3-only complexes. Constructs with two Cy3s show a minimum of three populations (one each for the Cy3s, one for the combined signal). We observe that the skipped constructs AB_{sk}0 show slightly reduced lifetime and brightness, possibly due to additional conformational flexibility and solvent exposure. The additional Cy3 on the bridge is also dimmer with a shorter lifetime, but clearly distinct from the AB_{sk}0 construct. The total AB_{in}0 signal is a near-perfect sum of the bridge Cy3 and the original ABO.

The A_cB0 construct is more complicated, likely due to base stacking or other conformational changes induced by the Cy3 at the 5' end of the A strand. A very dim population appears to correspond to the cap Cy3 only, as evidenced by transitions to and from the total A_cB0 signal population. The additional population is labeled with a “Q” because it appears to be a slightly quenched version of the A_cB0 population, although the reason for this population is not understood. We do not see FRETfluor signals for the A_cBN series that are consistent with the Q population acting as a donor; it is rarely seen.

All donor-only population means and standard deviations for brightness and 1-exp lifetime fits, along with the 2-exp lifetime fits for comparison, are provided in Supplementary Table S2. For the 2-exp lifetimes, photons from all levels in the 1-exp populations shown in the scatter plots were aggregated into a single decay for each data set, for which a 2-exp lifetime fit was performed. Lifetimes, standard deviations, and fractional populations are given for a set of fits across a minimum of seven data sets each (max 15); outliers would have been excluded but the 2-exp results were consistent and did not contain outliers.

Critically, we observe that τ and Φ indeed appear to vary independently for most Cy3-only populations. This is useful in the context of this work, as explained in Supplementary Note S5 and Supplementary Fig. S13, because this allows the FRET curve to be moved in different directions.

Supplementary Note S2: Raw trapping events

Supplementary Fig. S2 shows raw trapping events from a mixture including 27 FRETfluor labels. Most events contain a single state, but in cases where one donor blinks, additional states can be observed. Photophysical parameters within individual levels are generally stable over time. However, there are several events that can help us observe the photobleaching or blinking of either the donor or the acceptor. Transitions into and out of these blinking states are determined by the tag identity, and only “allowed” transitions are considered to be part of the same trapped event. In cases where non-allowed transitions are observed without a background level indicating an empty trap between events, it is likely that one trapped molecule was randomly replaced with another during the event. Here we highlight a few selected events to illustrate these effects:

For example, in the second row between 120-123 seconds, which shows an event from the tag AB8, the donor and acceptor are on during the event. Then, at 123 sec, the acceptor photobleaches, dropping the red brightness to nearly zero, and the green brightness level goes up. The new green-only level is consistent with the properties of the AB0 donor only construct as characterized in Supplementary Fig. S1.

Another example is the event in the first row at 15-25 seconds, which shows an event from the tag AB_{in}10, where both donors are on during the first part of the event. Then at 21 sec, the donor on the bridge blinks, leaving the red brightness the same and the green brightness lower than before. The spectroscopic information for the second part of this event is similar to an AB10 label. However, since there is no gap between these two states, we conclude that this blinking state also belongs to tag AB_{in}10.

In the second row at 62-70 seconds, the first part of the event shows both donors on A_cB10 are on, while the second part (at 65 sec) shows that the donor on the cap is off. This leaves the green brightness lower while the red brightness does not change much. The spectroscopic information for the second part of this event is also similar AB10. However, since the gap between these two states is extremely short, we also assign this level to tag A_cB10.

There are also several events indicating that there is very weak energy transfer between the second donor and the acceptor on the main strand. In the second row between 10-22 seconds, the first part of the event shows both donors and the acceptor for AB_{in}20 are all on while the second part (at 20 sec) shows that the donor on the bridge has blinked off. The photobleaching of the donor on the bridge leaves both the red and green brightness lower than before.

Supplementary Note S3: Sequence of the mRNA with binding site

The mRNA used in this work encodes the fluorescent protein eGFP, and includes proprietary tail sequences to help stabilize the mRNA against degradation. The sequence is given as follows:

```
[tail*]AUGGUGAGCAAGGGCGAGGAGCUGUUACCGGGGUGGUGGCCAUCCUGGUCGAGCUGGACGGC  
GACGUAAACGGCCACAAGUUCAGCGUGUCCGGCGAGGGCGAGGGCGAUGGCCACCUACGGCAAGCUGACCC
```

UGAAGUUCAUCUGCACCAACCAGGCAAGCUGCCGUGCCCUGGCCACCCUCGUGACCACCCUGACCUACGG
 CGUGCAGUGCUUCAGCGCUACCCGACCACAUGAAGCAGCACGACUUUCAAGUCCGCAUGCCGAA
 GGCUACGUCCAGGAGCGCACCAUCUUCUCAAGGACGACGGCAACUACAAGACCCGCGCCGAGGUGAAGU
 UCGAGGGCGACACCCUGGUGAACCGCAUCGAGCUGAAGGGCAUCGACUUCAAGGAGGACGGCAACAUCCU
 GGGCACAAGCUGGAGUACAAACAGCCACAACGUCUUAUCAUGGCCACAAGCAGAACAGGC
 AUCAAGGUGAACUUCAAGAUCCGCCACAACAUCAUCGAGGACGGCAGCGUGCAGCUCGCCACCACUACCAGC
 AGAACACCCCCAUCGGCGACGGCCCCGUGCUGCCGACAACCACUACCUGAGCACCCAGUCCGCCU
 GAGCAAAGACCCCAACGAGAACGCGCAUCACAUGGUCCUGUGAGUUCGUGACCGCCGGGAUCACU
 CUCGGCAUGGACGAGCUGUACAAGUAA [tail*]

*Proprietary tail sequences (TriLink BioTechnologies)

The secondary structure of the mRNA is predicted by RNAfold,^{2,3} and an image of this structure is shown in Supplementary Fig. S4. The target sequence is located in a high-confidence loop of the structure, highlighted here in gray and indicated on the structure shown in Supplementary Fig. S4 by the location of the FRETfluor binding.

Supplementary Note S4: Simulation of energy transfer between Cy3 and Cy5 on dsDNA

To model the expected magnitude of changes to different parameters in the spectroscopic output of FRETfluors due to changes in donor or acceptor photophysical properties, we created a simple model of FRET for doubly-tethered Cy3 and Cy5 on double-stranded DNA (dsDNA) after published works.⁴⁻⁶

Supplementary Fig. S13 shows the simple geometrical model of a rigid DNA double helix with doubly-tethered Cy3 and Cy5 incorporated into the backbone. B-form DNA parameters were taken from Ref 7. The diameter of the DNA is 2.37 nm, and the gap between base pairs is 0.34 nm (10 bp/turn). The distance between the DNA backbone and the fluorophore was set at 0.25 nm. The angular offset between the 3'-5' and the 5'-3' strand (-127°) is set by the minor groove height (1.2 nm) and helicity. For simplicity, we assumed that both dyes could rotate freely ($\kappa^2 = 2/3$).⁴ To create different constructs that were representative of different dye spacings in our FRETfluors, the Cy3 (donor) was kept at the same location for each construct and the Cy5 (acceptor) was moved to different locations along the opposite strand.

Dye photophysical parameters were assigned according to measured values when possible. For example, we measured the single-exponential fit to the lifetime decay for Cy3 doubly-tethered to the DNA backbone at the single molecule level as 1.6 ns, as shown in Supplementary Fig. S1. Other parameters: Cy5 lifetime (1.7 ns), quantum yields $\Phi_{\text{Cy3}} = 0.15$ and $\Phi_{\text{Cy5}} = 0.27$.^{8,9}

Briefly, we simulated a coupled energy transfer model where the time evolution of the probability of exciton residence on each fluorophore following absorption, $p = [p_{\text{Cy3}}(t), p_{\text{Cy5}}(t)]$ by one or the other fluorophore, $dp(t)/dt$, may be described by the master equation:

$$\frac{dp(t)}{dt} = \mathbf{M}p(t) \quad (3)$$

\mathbf{M} is an excitation transition matrix with off-diagonal elements representing the pairwise energy transfer rates, k_{ji} , (row i , column j) between donor j and acceptor i pigments. Entries on the diagonal indicate the total rate of energy loss at that fluorophore, including both energy transfer to the other pigments and the rate of fluorescent emission at that site, k_{ii}^{10} :

(4)

$$M_{ii} = - \left(k_{ii}^{10} + \sum_{i,j \neq i} k_{ji} \right)$$

To calculate initial values for the energy transfer rates, we used the Förster energy transfer equation^{4,10} using absorption and emission spectra for Cy3 and Cy5:

$$k_{DA} = \frac{k_D^{10} \Phi_D \kappa^2}{R_{DA}^6} \left(\frac{9000 \ln 10}{128\pi^5 N_A n^4} \right) \frac{\int Em_D \varepsilon_A \lambda^2 d\lambda}{\int Em_D \lambda^{-2} d\lambda} \quad (5)$$

For each initial condition $p(0) = [0, 1]$ and $p(0) = [1, 0]$, we can find the total probability of fluorescence emission from site i given excitation at site j by integrating over a long time (here: ~ 10 ns):

$$P_i^j \equiv \int_0^{+\infty} p_i^j(t) k_i^{10} \Phi_i dt \quad (6)$$

where Φ_i is the quantum yield of pigment i . The total probability of emission from fluorophore i given excitation at either fluorophore j , P_i^j , is then given according to the relative probabilities of each initial condition (determined by the absorbance probability at the excitation wavelength, 532 nm, for each fluorophore)

$$P_i = \sum_j A_j P_i^j \quad (7)$$

where A_j is the absorption probability at 532 nm for fluorophore j . The total probability of emission from fluorophore i , P_i , is directly proportional to the photon emission rate, or brightness B_i , from that fluorophore, by some unknown constant (*vide infra*). The predicted emission spectrum is a weighted sum of the individual fluorophore spectra, where the relative brightness of each pigment is used to weigh its contribution to the spectrum:

$$Em(\lambda) = \frac{\sum_i B_i Em_i(\lambda)}{\sum_i B_i} \quad (8)$$

This spectrum is separated into two spectral windows that encompass the red channel and the green channel, respectively. In order to allow our simulation results to be compared to measured data, we multiplied each brightness channel by the transmission profile of our emission filters (see *Methods*). In total, this translated to 71.43% throughput for the green channel, $Em(\text{green})$, and 46.18% throughput for the red channel, $Em(\text{red})$. Next, we scaled these unitless brightnesses to be comparable to our experimental brightness data for the ABN constructs using an approximate scaling factor (3 counts / 10 ms / μW). These became the simulation outputs for green and red channel brightnesses, “Green counts” and “Red counts” per Supplementary Fig. S13b (top panel).

As with our experimental data, FRET values (Supplementary Fig. S13b, bottom panel) were calculated according to an uncorrected ratio between the red channel and the sum over both channels:

$$FRET = \frac{\Sigma Em(\text{red})}{\Sigma Em(\text{red}) + \Sigma Em(\text{green})} \quad (9)$$

Finally, we predicted the observable single-exponential fluorescence lifetime of the donor by constructing the fluorescence decay of that state, $g_{donor}(t)$, and then fitting a single exponential decay function to find the apparent lifetime (see Supplementary Fig. S13b, bottom panel):

$$g_{donor}(t) = \sum_j k_i^{10} \Phi_i \left(\frac{\sum_j A_j p_i^j(t)}{\sum_j A_j} \right) \quad (10)$$

We calculated green and red brightness, green lifetime, and FRET values for complexes with spacings from 6 to 20 bp.

Supplementary Note S5: Effect of changing donor photophysical properties on FRET

We used our FRET simulation as described in Supplementary Note S4 above to model the expected magnitude of changes in spectroscopic signals we might measure for certain changes in photophysical properties of the donor Cy3. We separately modeled changes to the lifetime, τ , and quantum yield, Φ , of the donor, since our measurements of donor properties of different constructs indicated that changes in these variables across different constructs were not perfectly coupled (see Supplementary Note S1).

Per Supplementary Note S4, we experimentally observed donor brightnesses as low as 50% (for $A_{cap-only}B0$) compared to the brightest donor construct (AB0). A subtler reduction of ~15% brightness was observed for $AB_{sk}0$ as compared to AB0. Here, we take changes in brightness to reflect changes in quantum yield. For lifetimes, we observed reductions by up to a factor of three (for $A_{cap-only}B0$ as compared to AB0), and at minimum a 20% reduction ($AB_{sk}0$ as compared to AB0).

We modeled these minimal changes in Φ (15% reduction, red) and τ (20% reduction, green) using the simulation described in Supplementary Note S4 above to determine the predicted changes in our measured signals as compared to the original values (blue). As expected, both changes are most evident when FRET is low, and produce corresponding reductions in the observed brightness and lifetime for the lowest FRET states of approximately 15% and 20% for quantum yield and green lifetime, respectively (Supplementary Fig. S13b). We therefore expected that if populations with lower FRET could be clustered tightly within a few % or less, populations from the original constructs could be easily differentiated from the constructs with the modified donor properties.

These results also illustrate that the effects of changing Φ and τ are nearly orthogonal for the two data projections used throughout this work: The top panel is a brightness-brightness projection for the two color channels, while the bottom panel is a FRET- τ_{Green} projection. We note that the reduced Cy3 lifetime is apparent as a shifted green line only in the bottom panel of Supplementary Fig. S13b, and overlaps almost perfectly with the original blue line in the top panel (not shown due to overlap). Similarly, the reduced Cy3 quantum yield creates an obviously shifted red line top panel, but overlaps almost perfectly with the original blue line in the bottom panel.

In the three-dimensional view shows in Supplementary Fig. S13c, the near-orthogonality of these motions in $Gr-R-\tau$ space is clear. As discussed in Supplementary Note S4, traditionally Φ and τ are expected to be perfectly correlated under the assumption that the native radiative rate of a fluorophore does not change.¹ Here, our simulations illustrate the advantage of a situation where Φ and τ are not perfectly

coupled: independently changing donor properties can move the highly correlated FRET curve around the multidimensional parameter space, providing opportunities to create many distinct constructs.

References

1. Goldsmith, R. H. & Moerner, W. E. Watching conformational-and photodynamics of single fluorescent proteins in solution. *Nat. Chem.* **2**, 179–186 (2010).
2. Hofacker, I. L. Vienna RNA secondary structure server. *Nucleic Acids Res.* **31**, 3429–3431 (2003).
3. Lorenz, R. *et al.* ViennaRNA Package 2.0. *Algorithms Mol. Biol.* **6**, 26 (2011).
4. *Principles of Fluorescence Spectroscopy*. (Springer US, 2006). doi:10.1007/978-0-387-46312-4.
5. Wang, Q. & Moerner, W. E. Dissecting pigment architecture of individual photosynthetic antenna complexes in solution. *Proc. Natl. Acad. Sci.* **112**, 13880–13885 (2015).
6. Squires, A. H. *et al.* Single-molecule trapping and spectroscopy reveals photophysical heterogeneity of phycobilisomes quenched by Orange Carotenoid Protein. *Nat. Commun.* **10**, 1–12 (2019).
7. Bates, A. D. & Maxwell, A. *DNA topology*. (Oxford University Press, 2005).
8. Mujumdar, R. B., Ernst, L. A., Mujumdar, S. R., Lewis, C. J. & Waggoner, A. S. Cyanine dye labeling reagents: Sulfoindocyanine succinimidyl esters. *Bioconjug. Chem.* **4**, 105–111 (1993).
9. Sanborn, M. E., Connolly, B. K., Gurunathan, K. & Levitus, M. Fluorescence Properties and Photophysics of the Sulfoindocyanine Cy3 Linked Covalently to DNA. *J. Phys. Chem. B* **111**, 11064–11074 (2007).
10. Lerner, E. *et al.* FRET-based dynamic structural biology: Challenges, perspectives and an appeal for open-science practices. *eLife* **10**, e60416 (2021).